Dependence of Neuronal Correlations on Filter Characteristics and Marginal Spike Train Statistics

Tom Tetzlaff*
tom.tetzlaff@umb.no
Bernstein Center for Computational Neuroscience, Albert-Ludwigs-University,
D-79104 Freiburg, Germany, and Institute of Mathematical Sciences and Technology,
Norwegian University of Life Sciences, N-1432 Ås, Norway

Stefan Rotter
stefan.rotter@biologie.uni-freiburg.de
Bernstein Center for Computational Neuroscience, Albert-Ludwigs-University,
D-79104 Freiburg, Germany, and Theory and Data Analysis, Institute for Frontier
Areas of Psychology and Mental Health, D-79098 Freiburg, Germany

Eran Stark
eranst@ekmd.huji.ac.il
Department of Physiology, Hebrew University of Jerusalem, Jerusalem 91120, Israel

Moshe Abeles
abelesm@mail.biu.asc.il
Gonda Brain Research Institute, Bar Ilan University, Ramat-Gan 52900, Israel

Ad Aertsen
aertsen@biologie.uni-freiburg.de
Bernstein Center for Computational Neuroscience, and Neurobiology and Biophysics,
Faculty of Biology, Albert-Ludwigs-University, D-79104 Freiburg, Germany

Markus Diesmann
diesmann@brain.riken.jp
Bernstein Center for Computational Neuroscience, Albert-Ludwigs-University,
D-79104 Freiburg, Germany, and Brain Science Institute, RIKEN, Wako City,
Saitama 351-0198, Japan

Correlated neural activity has been observed at various signal levels (e.g., spike count, membrane potential, local field potential, EEG, fMRI BOLD). Most of these signals can be considered as superpositions of spike trains filtered by components of the neural system (synapses, membranes) and the measurement process. It is largely unknown how the

---

*Tom Tetzlaff is presently affiliated with the Norwegian University of Life Sciences.

spike train correlation structure is altered by this filtering and what the consequences for the dynamics of the system and for the interpretation of measured correlations are. In this study, we focus on linearly filtered spike trains and particularly consider correlations caused by overlapping presynaptic neuron populations. We demonstrate that correlation functions and statistical second-order measures like the variance, the covariance, and the correlation coefficient generally exhibit a complex dependence on the filter properties and the statistics of the presynaptic spike trains. We point out that both contributions can play a significant role in modulating the interaction strength between neurons or neuron populations. In many applications, the coherence allows a filter-independent quantification of correlated activity. In different network models, we discuss the estimation of network connectivity from the high-frequency coherence of simultaneous intracellular recordings of pairs of neurons.

1 Introduction

It has become a well-established belief among neuroscientists that fundamental knowledge of the function of the nervous system cannot be gained by looking at its individual elements without simultaneously describing their cooperative action. As a consequence, experimenters commonly perform parallel recordings of signals from different neurons, different neuron populations, or different brain areas. The detection and quantification of cooperative behavior in these data are frequently based on cross-correlation measures like the classical cross-correlation function (Perkel, Gerstein, & Moore, 1967b; Palm, Aertsen, & Gerstein, 1988), the joint peri stimulus time histogram (Aertsen, Gerstein, Habib, & Palm, 1989), or Pearson's correlation coefficient. A plethora of experimental studies demonstrated the existence of significant correlations in neuronal data at several signal levels, for various brain areas and different species, with distinct spatial and temporal characteristics and differently affected by varying stimulus conditions (Aertsen et al., 1989; Zohary, Shadlen, & Newsome, 1994; Vaadia et al., 1995; Lampl, Reichova, & Ferster, 1999; Bair, Zohary, & Newsome, 2001; Kohn & Smith, 2005; Mukamel et al., 2005; Sakurai & Takahashi, 2006).

Though the functional relevance of correlated neural activity is still under debate, the precise quantification and interpretation of neural correlations are with no doubt important for different fields of neuroscience. Spike count correlations, for example, have been thoroughly discussed in the context of coding by population rate since here correlations essentially limit the signal-to-noise ratio obtainable from a population of neurons (Zohary et al., 1994; Shadlen & Newsome, 1998). Depending on the population size, even tiny pairwise correlations can have substantial consequences for the precision of the population-averaged signal. Several authors (Abeles, 1991; Bienenstock, 1995; Hayon, Abeles, & Lehmann, 2004) highlight the potential benefit of correlated or synchronous spiking for the transmission and processing of

neural information. To assess the significance of observed precise firing patterns recurring in relation to the experimental protocol (Prut et al., 1998; Riehle, Grün, Diesmann, & Aertsen, 1997), it is essential to gain insight into the correlation structure already exhibited by network models serving as a null hypothesis. Further, several experimental and theoretical studies point out that the response of individual neurons can be effectively modulated by changing the strength of correlation between the synaptic inputs (Salinas & Sejnowski, 2000; Stroeve & Gielen, 2001; Rudolph & Destexhe, 2001; Oviedo & Reyes, 2002; Mikula & Niebur, 2003; Kuhn, Aertsen, & Rotter, 2003). Finally, the evaluation of the strength and the temporal characteristics of neuronal correlations under different stimulus conditions can shed light on details of the underlying network architecture (Aertsen et al., 1989; Bair et al., 2001; Kohn & Smith, 2005; Yoshimura & Callaway, 2005; Yoshimura, Dantzker, & Callaway, 2005). One of the major causes of correlated firing in neural networks is common presynaptic input. Depending on the underlying network architecture and the spatial organization of neurons, the size of the pool of common presynaptic sources varies. It is therefore tempting to relate identified common input correlations to network parameters. The present study shows, however, that this is not a trivial task even under simplifying assumptions like network homogeneity and stationarity.

Spiking activity is commonly considered as the computational basis of neural processing. Spike data, however, are represented in many different forms. The standard measure of spiking activity is the spike count: the number of observed spikes in a given time interval. Depending on the underlying question and method, the lengths of the time interval strongly differ in different studies and preparations. Measured spike trains, for example, are spike count signals at small timescales in the millisecond or submillisecond range. In many studies, spike counts are computed on larger timescales of several milliseconds, seconds, or even minutes (Bair et al., 2001; Kohn & Smith, 2005). Intracellular signals like membrane conductances, membrane currents, or membrane potentials are frequently considered as (linearly or nonlinearly) filtered versions of presynaptic spike signals. Similarly, extracellular local field potentials (LFP), electrocortico- (ECoG), or electroencephalography (EEG) data indirectly reflect compound spiking activity of neural populations. Even fMRI BOLD signals were shown to be related to filtered spiking activity (Mukamel et al., 2005). Significant correlations in neuronal data have been found at all signal levels: multi-unit spike activity (MUA) (Eckhorn et al., 1988; Singer, Gray, Engel, & König, 1988; Gray & Singer, 1989; Gray, König, Engel, & Singer, 1989; Gray, 1994), single-unit spike activity (SUA) (Aertsen et al., 1989; Zohary et al., 1994; Vaadia et al., 1995; Lampl et al., 1999; Sakurai & Takahashi, 2006), spike counts at different timescales (SUA) (Bair et al., 2001; Kohn & Smith, 2005), membrane potentials (Lampl et al., 1999), LFP (Fries, Reynolds, Rorie, & Desimone, 2001; Logothetis, Pauls, Augath, Trinath, & Oeltermann, 2001; Mukamel et al., 2005), EEG (Shaw, 1984; French & Beaumont, 1984; Weiss & Mueller,

2003), and fMRI (Logothetis et al., 2001; Hasson, Nir, Levy, Fuhrmann, & Malach, 2004; Mukamel et al., 2005). Several studies investigated the relation between different types of signals using correlation measures (Logothetis et al., 2001; Mukamel et al., 2005).

In this study, we address the question how traditional correlation measures are altered by linear filtering and emphasize the consequences for the interpretation of those measures with respect to neural dynamics and network structure. We show that the interplay between the spike train auto- and cross-correlation structure and the filter properties determines the magnitude and the temporal features of correlations observed by the experimenter or the neural system itself. For illustration, consider the scenario in Figure 1A. Here, two neurons i and j receive an excitatory input spike train $\xi_c(t)$ from a common pool of presynaptic neurons and uncorrelated Poissonian spike trains $\xi_{d_{i/j}}(t)$ from disjoint sources. The membrane potentials $x_i(t)$, $x_j(t)$ of the two neurons i and j are modeled by low-pass filtering of the compound spike trains $\xi_{i/j}(t) = \xi_c(t) + \xi_{d_{i/j}}$ with an exponential kernel $f(t) \sim \exp(-t/\tau_m)$ (see Figure 1B). The firing rates of the common and the two disjoint spike trains are identical and do not change over time. Thus, the ratio between the expected number of common spikes and the total number of spikes in each process is 0.5. Nevertheless, the measured correlation coefficient between the corresponding membrane potentials shown in Figure 1B suddenly decreases from 0.5 to about 0.3 at time $t = 1024$ ms (see Figure 1C). The reason for this change in the correlation coefficient is a modulation of the second-order interval statistics of the common source $\xi_c(t)$. While its interspike interval distribution is exponential (Poisson process) in the first half of the experiment ($t \leq 1024$ ms), interspike intervals are drawn from a gamma distribution of order $\gamma = 5$ in the second part ($t > 1024$ ms). The mean interspike interval is kept constant throughout the whole simulation. The example points out that the correlation coefficient of the filtered spike trains generally depends not only on the joint but also on the marginal second-order statistics of the spike trains. In the course of this article, we demonstrate that the coherence between the two signals at high frequencies is under certain conditions insensitive to the latter and thus can be used to measure the common-input strength in a more reliable way (see Figure 1C).

In section 2 we show how the structure of the shot-noise correlation functions and second-order measures like variance, covariance, and correlation coefficient depend on the features of the chosen filter kernel and the spike train statistics in general. In the remainder of the article, we apply these results to the specific class of correlations arising from shared presynaptic sources in a basic common-input scenario (see section 3), in a stochastic model of a small cortical volume (see section 4), and finally in a random network of excitatory and inhibitory integrate-and-fire neurons (see section 5).

Preliminary results have been presented in abstract form (Tetzlaff, Aertsen, & Diesmann, 2005).
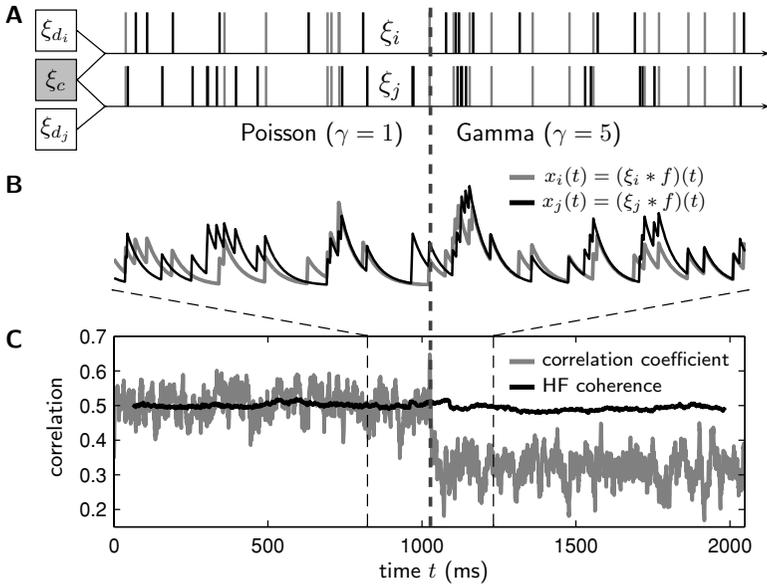
Figure 1: Time dependence of the membrane potential correlation coefficient induced by a change in marginal spike train statistics. (A) Sketch of two correlated model spike trains $\xi_i(t)$, $\xi_j(t)$ constructed by merging spikes from a common source $\xi_c(t)$ (gray bars) and two disjoint independent Poissonian sources $\xi_{d_i}(t)$ and $\xi_{d_j}(t)$ (black bars). During the first half of the simulation ($t < 1024\,\text{ms}$), the common source $\xi_c(t)$ is modeled as a Poisson process (exponential interspike interval distribution). In the second half ($t > 1024\,\text{ms}$), its interspike intervals are drawn from a gamma distribution of order $\gamma = 5$. The mean interspike interval is kept constant at $20\,\text{ms}$ throughout the simulation (rate of the common source $\nu_c = 50\,\text{s}^{-1}$, rate of the disjoint sources $\nu_d = 50\,\text{s}^{-1}$, total simulation time $T = 2048\,\text{ms}$). The model spike trains $\xi_i(t)$ and $\xi_j(t)$ are considered as the superpositions of excitatory inputs to two neurons i and j, respectively. (B) Membrane potentials $x_i(t)$ and $x_j(t)$ obtained by low-pass filtering of the spike trains $\xi_i(t)$ and $\xi_j(t)$ shown in A with an exponential kernel $f(t)$ (time constant $\tau_m = 10\,\text{ms}$). (C) Time-resolved correlation coefficient (gray curve) of the membrane potentials and average high-frequency ($0.3, \ldots, 1\,\text{kHz}$) coherence (black curve, see section 3.4) derived from power- and cross-spectra of the membrane potentials measured in a sliding window of width $128\,\text{ms}$, both averaged over 500 realizations.

2 Shot-Noise Correlations in the Time and Frequency Domain

This section provides the formalism used in the remainder of this article and derives the relations between point-process (spike train) correlations and correlations of continuous signals resulting from the point processes by

linear filtering (shot noise). The results presented in sections 2.1 and 2.2 are generalizations of those outlined in for example Papoulis and Pillai (2002) for the second-order marginal statistics of shot-noise signals.

2.1 Correlation Functions and Correlation Coefficient. In the following, we focus on signals $x_i(t)$ constructed from spike trains $\xi_i(t)$ by convolution ($*$) with some time-invariant kernel $f_i(t)$ (linear filtering):[1]

$$x_i(t) := (\xi_i * f_i)(t) = \int_{-\infty}^{\infty} ds\ \xi_i(s) f_i(t - s). \tag{2.1}$$

In the literature, $x_i(t)$ is commonly called shot noise if $\xi_i(t)$ is a realization of a Poisson point process (Papoulis & Pillai, 2002). Here we adopt this term for general point processes. Various measures in theoretical and experimental neuroscience can be described as shot noise. The subthreshold membrane potential of the linear integrate-and-fire neuron model with current-based synapses (Tuckwell, 1988), for example, is simply the convolution of the incoming spike trains with the postsynaptic potentials (PSPs). It has been shown that population signals like local field potentials (LFPs), EEG, and even fMRI (BOLD) signals exhibit a considerable correlation with linearly filtered spike data (Logothetis et al., 2001; Mukamel et al., 2005). Also the frequently used spike count measure, the number of spikes occurring in a finite time window $[t, t + h)$, is a shot-noise signal (see section 2.3).

We define the two-dimensional spike train and shot-noise correlation functions $\psi_{ij}(t, t') := E[\xi_i(t)\xi_j(t')]$ and $c_{ij}(t, t') := E[x_i(t)x_j(t')]$, respectively, as the expected[2] products of the two spike trains $\xi_i(t)$, $\xi_j(t')$ and the two shot-noise signals $x_i(t)$, $x_j(t')$ evaluated at times t and t' (Aertsen et al., 1989). Offset subtraction, $\tilde{\xi}_i(t) := \xi_i(t) - \nu_i(t)$ and $\tilde{x}_i(t) := x_i(t) - (\nu_i * f_i)(t)$, yields the corresponding covariance functions

$$\begin{aligned} \tilde{\psi}_{ij}(t, t') &:= E[\tilde{\xi}_i(t)\tilde{\xi}_j(t')], \\ \tilde{c}_{ij}(t, t') &:= E[\tilde{x}_i(t)\tilde{x}_j(t')]. \end{aligned} \tag{2.2}$$

Here, $\nu_i(t) := E[\xi_i(t)]$ denotes the instantaneous rate of the process $\xi_i(t)$. According to equations 2.1 and 2.2, the shot-noise and spike train covariance functions are linked by a two-dimensional convolution with the filter

---

[1]Throughout this article, we refer to a specific spike train realization $\xi_i(t)$ as a sum over delta functions centered at the spike times t_i^k: $\xi_i(t) := \sum_k \delta(t - t_i^k)$. The abstract quantity "spike train" can be considered as being derived from the observable quantity "spike count" $x_i^h(t)$—the number of spikes occurring in the time interval $[t, t + h)$—by taking the limit $h \to 0$: $\xi_i(t) = \lim_{h \to 0} \frac{1}{h} x_i^h(t)$.

[2]Here, $E[\cdot]$ denotes an average over realizations (trials).

kernels $f_i(t)$ and $f_j(t)$:

$$\tilde{c}_{ij}(t, t') = \int_{-\infty}^{\infty} ds \int_{-\infty}^{\infty} ds' \ \tilde{\psi}_{ij}(s, s') f_i(t - s) f_j(t' - s'). \tag{2.3}$$

Assuming time invariance of $\tilde{\psi}_{ij}(t, t')$ (second-order stationarity), we obtain the one-dimensional shot-noise covariance function (Papoulis & Pillai, 2002),

$$\tilde{c}_{ij}(\tau) := \tilde{c}_{ij}(t, t + \tau) = (\tilde{\psi}_{ij} * \phi_{ij})(\tau), \tag{2.4}$$

as a convolution between the one-dimensional spike train covariance function,

$$\tilde{\psi}_{ij}(\tau) := \tilde{\psi}_{ij}(t, t + \tau) = \tilde{\psi}_{ij}(0, \tau) \qquad (\forall t, \ \tau), \tag{2.5}$$

and the (deterministic) cross-correlation $\phi_{ij}(\tau) := \int_{-\infty}^{\infty} dt \ f_i(t) f_j(t + \tau)$ of the two filter kernels $f_i(t)$ and $f_j(t)$.

The shot-noise covariance $\tilde{c}_{ij}$ (or variance for $i = j$) is obtained by evaluating the covariance function $\tilde{c}_{ij}(\tau)$ at zero lag $\tau = 0$. According to equation 2.4, this is the area of the product of the spike train covariance function and the filter correlation function:

$$\tilde{c}_{ij} := \tilde{c}_{ij}(0) = \int_{-\infty}^{\infty} dt \ \tilde{\psi}_{ij}(t) \phi_{ij}(-t). \tag{2.6}$$

For signals $x_i(t)$, $x_j(t)$ with finite variance, the covariance can be normalized by the fluctuations of the individual signals to the scale $[-1, 1]$. This defines Pearson's correlation coefficient (Perkel, Gerstein, & Moore, 1967b; Hollander & Wolfe, 1999; Feller, 1971):

$$r_{ij} := \frac{\tilde{c}_{ij}}{\sqrt{\tilde{c}_{ii}\tilde{c}_{jj}}} = \frac{\int_{-\infty}^{\infty} dt \ \tilde{\psi}_{ij}(t)\phi_{ij}(-t)}{\sqrt{\int_{-\infty}^{\infty} dt \ \tilde{\psi}_{ii}(t)\phi_{ii}(t) \int_{-\infty}^{\infty} dt' \ \tilde{\psi}_{jj}(t')\phi_{jj}(t')}}. \tag{2.7}$$

Note that r_{ij} generally depends on both the (joint and marginal) statistics of the underlying spike trains and the features of the filter kernels, even if the kernels $f_i(t)$ and $f_j(t)$ are identical: $\phi_{ij}(t) = \phi_{ii}(t) = \phi_{jj}(t)$. Only if, in addition, all spike train covariance functions $\tilde{\psi}_{ii/jj/ij}(\tau)$ are delta shaped (e.g., precisely correlated, stationary Poisson processes), the filter contributions cancel out.

2.2 Spectra and Coherence. Correlations in or between time series are often considered not only in the time but also in the Fourier (frequency)

domain. If we denote $\Xi_i(\omega)$ and $F_i(\omega)$ as the Fourier transforms[3] of the spike train $\xi_i(t)$ and the filter kernel $f_i(t)$, respectively, the Fourier transform of the shot noise $x_i(t)$, defined in equation 2.1, reads $X_i(\omega) = \Xi_i(\omega)F_i(\omega)$. Given the one- and two-dimensional spike train spectra,[4]

$$\check{\Psi}_{ij}(\omega, \omega') := \mathfrak{F}[\check{\psi}_{ij}(t, t')](\omega, \omega') \quad \text{and} \quad \check{\Psi}_{ij}(\omega) := \mathfrak{F}[\check{\psi}_{ij}(\tau)](\omega), \quad (2.8)$$

we obtain

$$\tilde{C}_{ij}(\omega, \omega') = \check{\Psi}_{ij}(\omega, \omega')F_i(\omega)F_j(\omega') \quad \text{and} \quad \tilde{C}_{ij}(\omega) = \check{\Psi}_{ij}(\omega)\Phi_{ij}(\omega) \quad (2.9)$$

as the one- and two-dimensional power- ($i = j$) and cross-spectra ($i \neq j$) of the shot-noise signals by Fourier-transforming equations, 2.3 and 2.4, respectively. $\Phi_{ij}(\omega) := F_i(\omega)F_j^*(\omega)$ in equation 2.9 denotes the the power- ($i = j$) or cross-spectrum ($i \neq j$) of the filter kernels $f_i(t)$ and $f_j(t)$ (the superscript * represents the complex conjugate).

A normalized correlation measure in the frequency domain is the complex coherence (Priestley, 1983; Jarvis & Mitra, 2001),

$$\kappa'_{ij}(\omega) := \frac{\tilde{C}_{ij}(\omega)}{\sqrt{\tilde{C}_{ii}(\omega)\tilde{C}_{jj}(\omega)}} = \frac{\check{\Psi}_{ij}(\omega)\Phi_{ij}(\omega)}{\sqrt{\check{\Psi}_{ii}(\omega)\check{\Psi}_{jj}(\omega)\Phi_{ii}(\omega)\Phi_{jj}(\omega)}}, \quad (2.10)$$

which is defined as the ratio between the cross-spectrum $\tilde{C}_{ij}(\omega)$ and the geometric mean of the power spectra $\tilde{C}_{ii/jj}(\omega)$. Its modulus (amplitude) $\kappa(\omega) := |\kappa'(\omega)|$, restricted to the range $[0, 1]$, is called coherence. The phase of the complex coherence, equation 2.10, contains information about the temporal alignment of the two signals $x_i(t)$ and $x_j(t)$ and can therefore be used to study delays or negative correlations (anticorrelations). Note that the definition of the coherence is meaningful only at frequencies with nonvanishing power.

With $\Phi_{ij}(\omega) = F_i(\omega)F_j^*(\omega)$, it is straightforward to see that the coherence $\kappa(\omega)$ is, in contrast to the correlation coefficient r_{ij} in equation 2.7, independent of the linear filter kernels $f_{i/j}(t)$ and exclusively reflects the statistical properties of the spike trains (Brown, Kaas, & Mitra, 2004):

$$\kappa(\omega) = \frac{|\check{\Psi}_{ij}(\omega)|}{\sqrt{\check{\Psi}_{ii}(\omega)\check{\Psi}_{jj}(\omega)}} \quad \text{(for any } f_i(t) \text{ and } f_j(t)\text{).} \quad (2.11)$$

---

[3]Throughout the article, Fourier transforms are represented by capital letters.
[4]$\mathfrak{F}[\cdot](\omega, \omega')$ and $\mathfrak{F}[\cdot](\omega)$ denote the two- and one-dimensional Fourier integrals, respectively.

However, this does not hold if the shot-noise signals arise from superpositions $x_i(t) = \sum_{k=1}^{n}(\xi_k * f_{ik})(t)$ of n spike trains convolved with different kernels $f_{ik}(t)$. In this case, the spectra read $\tilde{C}_{ij}(\omega) = \sum_k \sum_l \tilde{\Psi}_{kl}(\omega) F_{ik}(\omega) F_{jl}^*(\omega)$. In general, the resulting coherence is filter independent only if the kernels $f_{ik}(t)\,(k \in [1, n])$ are identical.

Note that $\kappa'(\omega)$ evaluated at frequency $\omega = 0$ is the area of the covariance function normalized by the areas of the autocovariance functions:

$$\kappa'(0) = \frac{\int_{-\infty}^{\infty} d\tau\, \tilde{c}_{ij}(\tau)}{\sqrt{\int_{-\infty}^{\infty} d\tau\, \tilde{c}_{ii}(\tau) \int_{-\infty}^{\infty} d\tau'\, \tilde{c}_{jj}(\tau')}}. \tag{2.12}$$

In the neuroscientific context $\kappa'(0)$ is frequently called *correlation coefficient* too (Bair et al., 2001; Kohn & Smith, 2005; Moreno-Bote & Parga, 2006). The motivation to prefer $\kappa'(0)$ over r_{ij} in these works is the observation that peaks in neuronal correlation functions typically have some temporal extent and that the width of the peaks varies depending on the system and the experimental protocol. Therefore, an integrated measure appears adequate. Our considerations above demonstrate an additional advantage of $\kappa'(0)$: it is independent of a joint shot-noise kernel. In this article, we reserve the term *correlation coefficient* for r_{ij} as defined in equation 2.7.

2.3 Example: Spike Count. Before we investigate models of neuronal correlation in the next sections, let us first turn to a shot-noise process not originating from the biophysical properties of the system but from the measurement process itself: the spike count:

$$x_i^h(t) := \int_t^{t+h} ds\, \xi_i(s), \tag{2.13}$$

that is, the number of spikes observed in a time window $[t, t + h)$. The measure can be viewed as resulting from the convolution of the spike train $\xi_i(t)$ with the rectangular kernel,

$$f_i(t) = \begin{cases} 1 & -h < t \leq 0 \\ 0 & \text{else} \end{cases}. \tag{2.14}$$

In many applications the spike count is computed on a discrete time grid $t \in \{k \cdot h | k \in \mathbb{N}\}$, whereas here, we consider the general case of continuous time where spikes are counted in a sliding window (moving average). The results of this section are formally the same for both the continuous and the discrete case. In the latter, time integrals (convolutions) have to be replaced by sums over time steps.

For simplicity, we restrict ourselves to the case of identical filter kernels $f(t) := f_i(t) = f_j(t)$ and therefore $\phi(\tau) := \phi_{ii}(\tau) = \phi_{jj}(\tau) = \phi_{ij}(\tau)$. Utilizing equation 2.6, we obtain the spike count covariance,

$$\tilde{c}_{ij}^h = \int_{-h}^{h} d\tau \, (h - |\tau|) \cdot \tilde{\psi}_{ij}(\tau), \tag{2.15}$$

for a given spike train covariance function $\tilde{\psi}_{ij}(\tau)$ and a bin width h. The integration limits $[-h, h]$ and the prefactor $(h - |\tau|)$ result from the autocorrelation[5] of $f(t)$:

$$\phi(\tau) = \int_{-\infty}^{\infty} dt \, f(t)f(t+\tau) = \begin{cases} h - |\tau| & -h < \tau \le h \\ 0 & \text{else} \end{cases}. \tag{2.16}$$

For $i = j$, equation 2.15 resembles the result for the spike count variance presented in Papoulis and Pillai (2002). The spike count correlation coefficient,

$$r_{ij}^h := \frac{\tilde{c}_{ij}^h}{\sqrt{\tilde{c}_{ii}^h \tilde{c}_{jj}^h}} = \frac{\int_{-h}^{h} d\tau \, (h - |\tau|) \, \tilde{\psi}_{ij}(\tau)}{\sqrt{\int_{-h}^{h} d\tau \, (h - |\tau|) \, \tilde{\psi}_{ii}(\tau) \int_{-h}^{h} d\tau' \, (h - |\tau'|) \, \tilde{\psi}_{jj}(\tau')}}, \tag{2.17}$$

is, up to the triangular prefactors $(h - |\tau|)$, the normalized area of the spike train cross-covariance function in the interval $[-h, h]$. Bair et al. (2001) studied the timescale dependence of spike count correlations using this measure but omitted the triangular prefactors.

Consider the simple example of a single stationary Poisson process with constant rate ν_i and autocovariance function (Papoulis & Pillai, 2002)

$$\tilde{\psi}_{ii}(\tau) = \nu_i \delta(\tau). \tag{2.18}$$

---

[5]If $f_i(t) \ne f_j(t)$ and assuming $h_i < h_j$, $\phi(\tau)$ has to be replaced by the filter cross-correlation:

$$\phi_{ij}(\tau) = \begin{cases} 0 & \tau \le -h_j \\ h_j + \tau & -h_j < \tau \le -(h_j - h_i) \\ h_i & -(h_j - h_i) < \tau \le 0 \\ h_i - \tau & 0 < \tau \le h_i \\ 0 & \tau > h_i \end{cases}.$$

Applying equation 2.15 immediately recovers the well-known result for the spike count variance of a Poisson process,

$$\tilde{c}_{ii}^{h} = v_i \int_{-h}^{h} d\tau \ (h - |\tau|) \cdot \delta(\tau) = v_i h, \tag{2.19}$$

with a linear dependence on the bin size h. A similar result is obtained for the count covariance of two processes with delta-shaped cross-covariance function. Natural spike trains, however, typically exhibit structured covariance functions. It is a major objective of this article to point out that the natural nondelta-type correlation structure leads to a complex dependence of correlation coefficients on the properties of the filter kernels.

3 The Common Input Scenario

Equipped with the formalism to study the correlation between two shot-noise signals developed in the previous section, we investigate in this section how non-Poissonian spike statistics and nonstationary firing rates affect pairwise correlations between filtered spike trains in common input models. To this end, we define a minimal structural model describing two neurons sharing part of their inputs (see section 3.1) and derive the resulting spike train correlation functions (see section 3.2). Section 3.3 exploits the results of section 2.1 to calculate the variance, the covariance, and the correlation coefficient of spike count signals for two examples introduced in sections 3.2.1 and 3.2.2. In section 3.2.1, a gamma process is considered to highlight how measured correlations depend on the autocorrelation of the common source. An inhomogeneous Poisson processes with sinusoidal rate modulation in time and random phase across trials (see section 3.2.2) is employed to clarify the notion of nonstationarity in the context of the correlation coefficient. Section 3.4 demonstrates that for a large class of processes, the high-frequency coherence reflects the common input strength and therefore provides an unambiguous measure that depends on neither the filter nor the marginal statistics of the presynaptic sources. Section 3.5 is concerned with the natural situation where spike cross-correlations exhibit a temporal dispersion as originating from heterogeneous delays, a finite rise time of the postsynaptic potentials, or other mechanisms.

3.1 Model Definition. Two spike trains $\xi_i(t)$ and $\xi_j(t)$, constituting the total presynaptic activity of two neurons i and j, are constructed by superimposing two disjoint processes $\xi_{d_i}(t)$ and $\xi_{d_j}(t)$ with a process $\xi_c(t)$ shared by both neurons:

$$\xi_i(t) = \xi_{d_i}(t) + \xi_c(t), \quad \xi_j(t) = \xi_{d_j}(t) + \xi_c(t) \tag{3.1}$$

(see Figure 1A for an illustration of the architecture). To reduce the number of parameters, we assume that the rates of $\xi_i(t)$ and $\xi_j(t)$ are identical, $\nu(t) := \nu_i(t) = \nu_j(t)$. The strength of the common source is parameterized by the relative contribution $\alpha := \nu_c(t)/\nu(t)$ of its firing rate to the total rate. The rates of the background processes $\xi_{d_i}(t)$ and $\xi_{d_j}(t)$ can thus be expressed as $\nu_d(t) := \nu_{d_i}(t) = \nu_{d_j}(t) = (1 - \alpha)\nu(t)$.

3.2 Correlation Functions. The (one-dimensional) auto- and cross-covariance functions of the two (centered) spike trains $\tilde{\xi}_i(t)$ and $\tilde{\xi}_j(t)$ are

$$\tilde{\psi}_{ii}(\tau) = E[\tilde{\xi}_i(t)\tilde{\xi}_i(t + \tau)] = \tilde{\psi}_{d_id_i}(\tau) + \tilde{\psi}_{d_ic}(\tau) + \tilde{\psi}_{cd_i}(\tau) + \tilde{\psi}_{cc}(\tau) \quad (3.2)$$

$$\tilde{\psi}_{ij}(\tau) = E[\tilde{\xi}_i(t)\tilde{\xi}_j(t + \tau)] = \tilde{\psi}_{d_id_j}(\tau) + \tilde{\psi}_{d_ic}(\tau) + \tilde{\psi}_{cd_j}(\tau) + \tilde{\psi}_{cc}(\tau). \quad (3.3)$$

Obviously both are generally determined by the marginal as well as the joint second-order statistics of the presynaptic sources. Let us, again for the sake of simplicity, assume that the disjoint and the common processes are mutually uncorrelated:

$$\tilde{\psi}_{d_id_j}(\tau) = \tilde{\psi}_{d_ic}(\tau) = \tilde{\psi}_{d_jc}(\tau) = 0. \quad (3.4)$$

In this case, equations 3.2 and 3.3 reduce to

$$\tilde{\psi}_{ii}(\tau) = \tilde{\psi}_{d_id_i}(\tau) + \tilde{\psi}_{cc}(\tau) \quad (3.5)$$

$$\tilde{\psi}_{ij}(\tau) = \tilde{\psi}_{cc}(\tau). \quad (3.6)$$

The disjoint inputs are modeled as stationary Poissonian sources with constant firing rate ν_d, hence

$$\tilde{\psi}_{d_id_i}(\tau) = \nu_d \delta(\tau). \quad (3.7)$$

In order to dissect the effect of different aspects of the common source process $\xi_c(t)$ on common input correlations, we investigate two specific cases. The stationary gamma process (see section 3.2.1) is discussed as a simple example of a non-Poissonian point process in order to demonstrate how common input correlations are altered by the interval distribution of the common source process. The effect of nonstationarity in time and across trials on common input correlations is discussed by considering the common source process as an inhomogeneous Poisson process with random rate (see section 3.2.2).

3.2.1 *Gamma Source.* Let the common source emit spikes at intervals drawn from a gamma distribution,

$$p_1(\tau) = v_c \gamma \frac{(v_c \gamma \tau)^{\gamma - 1}}{(\gamma - 1)!} \exp(-v_c \gamma \tau), \tag{3.8}$$

with positive integer orders $\gamma \in \mathbb{N}^+$. The autocorrelation function of a general point process is determined by the sum over all kth-order interval distributions $p_k(\tau)$ (Perkel, Gerstein, & Moore, 1967a):

$$\psi_{cc}(\tau) = v_c \left(\delta(\tau) + \sum_{k=1}^{\infty} p_k(|\tau|) \right). \tag{3.9}$$

For any renewal process, consecutive intervals are independent (Cox, 1962). Therefore, $p_k(\tau)$ is the k-fold convolution of the first-order density,

$$p_k(\tau) = \underbrace{(p_1 * \cdots * p_1)}_{k}(\tau). \tag{3.10}$$

As equation 3.10 factorizes in the Fourier domain, $P_k(\omega) = P_1(\omega)^k$, the power spectrum of a renewal process reads

$$
\begin{aligned}
\Psi_{cc}(\omega) &= \mathfrak{F}\left[\psi_{cc}(\tau)\right](\omega) \\
&= v_c \left(1 + \sum_{k=1}^{\infty} \left\{ P_1(\omega)^k + P_1^*(\omega)^k \right\} \right) \\
&= v_c \left(1 - 2 + \sum_{k=0}^{\infty} \left\{ P_1(\omega)^k + P_1^*(\omega)^k \right\} \right) \\
&= v_c \left([1 - P_1(\omega)]^{-1} + [1 - P_1^*(\omega)]^{-1} - 1 \right).
\end{aligned}
\tag{3.11}
$$

The Fourier-transformed first-order interval density of the gamma process is given by (Cox, 1962)

$$P_1(\omega) = \mathfrak{F}\left[p_1(t)\right](\omega) = \left(\frac{\gamma v_c}{\gamma v_c + \omega} \right)^{\gamma}. \tag{3.12}$$

The autocorrelation function $\psi_{cc}(\tau)$ can now be obtained by (numerically) computing the inverse Fourier transform of the spectrum, equation 3.11. A closed analytical expression for the autocovariance function can also be

derived by a direct evaluation of equation 3.9:[6]

$$\tilde{\psi}_{cc}(\tau) = \nu_c \delta(\tau) + \nu_c^2 \sum_{l=1}^{\gamma-1} e^{2\pi i l/\gamma} \exp(\gamma \nu_c \tau [e^{2\pi i l/\gamma} - 1]). \qquad (3.13)$$

Gamma processes are frequently considered as models of neuronal firing since they can mimic the refractory behavior of neurons following spike emission. For $\gamma > 1$, short interspike intervals become more and more unlikely. This is reflected in the autocovariance functions, which exhibit a trough around the central peak at $\tau = 0$ (see Figure 2A, left). A limitation of the choice of gamma processes is their tendency to become more and more regular with the coefficient of variation scaling as $1/\sqrt{\gamma}$ (Cox, 1962). Observed coefficients of variation in cortical spike trains, however, remain close to one (Softky & Koch, 1993).

3.2.2 Inhomogeneous Poisson Source. In a second example we model the common source as a doubly stochastic process (Cox process; see Daley & Vere-Jones, 2005) where not only the spike train realizations l but also the rate profiles are random. In the kth trial, $\xi_c^l(t|k)$ is considered as a realization of a Poisson process with a time-dependent rate function $\nu_c^k(t) := E_l[\xi_c^l(t|k)]$ and autocorrelation (Papoulis & Pillai, 2002):

$$\psi_{cc}^k(t, t') := E_l \left[\xi_c^l(t \mid k) \xi_c^l(t' \mid k) \right] = \nu_c^k(t) \delta(t - t') + \nu_c^k(t) \nu_c^k(t'). \qquad (3.14)$$

Across trials, the firing rate profiles $\nu_c^k(t)$ change randomly. In the following, all expectation values $E[\cdot]$ therefore have to be interpreted as expectations over realizations l and over trials k, that is, $E[\cdot] = E_k[E_l[\cdot]]$. After averaging over k, the covariance function reads

$$\tilde{\psi}_{cc}(t, t') = E_k \left[\nu_c^k(t) \right] \delta(t - t') + \tilde{\gamma}_{cc}(t, t'), \qquad (3.15)$$

with

$$\tilde{\gamma}_{cc}(t, t') = E_k \left[\nu_c^k(t) \nu_c^k(t') \right] - E_k \left[\nu_c^k(t) \right] E_k \left[\nu_c^k(t') \right] \qquad (3.16)$$

being the autocovariance function of the firing rate. If the rate functions were identical in each trial, averaging over k would not have any effect; the two terms in equation 3.16 would cancel out, and in equation 3.15, only the delta peak would remain. In all other cases, however, the rate covariance

---

[6]For a derivation, see Pipa, van Vreeswijk, and Grün (2008).

function $\tilde{\gamma}_{cc}(t, t')$ determines the structure of the spike train covariance function.

In order to study the interplay between nonstationarity in time and nonstationarity across trials, it is sufficient to restrict the discussion to processes where the average firing rate is constant in time,

$$E_k \left[v_c^k(t) \right] =: v_c. \tag{3.17}$$

At first sight, this seems to imply simultaneous stationarity of the spike-generating process in time and across trials. Thus, for any given trial k, we would expect the firing rate describing the process to be constant in time $v_c^k(t) = v_c^k$, and for any given point in time t, we would expect the firing rate to be constant across trials $v_c^k(t) = v_c(t)$. In fact, however, stationarity in time follows only if, in addition to equation 3.17, the system is stationary across trials. Consider, as an example, a process with sinusoidal rate function and stationary frequency $f_0 = \omega_0/2\pi$, but phase $\phi_k \in [0, 2\pi)$ uniformly distributed across trials:

$$v_c^k(t) = v_c[1 + \cos(\omega_0 t + \phi_k)]. \tag{3.18}$$

Averaging over the ensemble of trials (k) results in a constant value $v_c = E_k[v_c^k(t)]$ despite the nonstationary firing rate driving spike generation in each individual trial. Thus, by construction of the process, the trial-averaged firing rate does not expose any underlying nonstationarity. In contrast, the trial-averaged autocovariance function does. The rate covariance function is given by

$$\tilde{\gamma}_{cc}(t, t') = \frac{1}{2} v_c^2 \cos(\omega_0[t - t']) \tag{3.19}$$

and depends on only the time difference $\tau = t - t'$. Hence, we obtain for the spike train covariance function of the common source,

$$\tilde{\psi}_{cc}(\tau) = v_c \delta(\tau) + \frac{1}{2} v_c^2 \cos(\omega_0 \tau). \tag{3.20}$$

The fact that the two-dimensional correlation function $\tilde{\psi}_{cc}(t, t')$ is time invariant allows us to compute the one-dimensional shot-noise correlations using equation 2.4 in the subsequent sections.

3.3 Bin Size and Autocorrelation Dependence of Spike Count Correlations. With a generic correlation model at hand, we can now discuss how measured correlations depend on the choice of the filter kernel and the marginal statistics of the presynaptic sources parameterized by the γ-order

in the first example (in section 3.2.1) and by the oscillation frequency ω_0 in the Poisson example (in section 3.2.2).

With equation 2.15 and the spike train autocovariance function $\tilde{\psi}_{cc}(\tau)$ of the common sources given by equations 3.13 and 3.20, we obtain for the spike count covariance of the gamma example,

$$\tilde{c}_{ij}^h = \nu_c h + 2 \sum_{l=1}^{\gamma-1} \frac{A_l}{B_l} (h - B_l^{-1}[1 - e^{-B_l h}]), \tag{3.21}$$

where $A_l = \nu_c^2 e^{2\pi i l / \gamma}$ and $B_l = \gamma \nu_c (1 - e^{2\pi i l / \gamma})$, and for the oscillating Poisson example,

$$\tilde{c}_{ij}^h = \nu_c h - \frac{\nu_c^2}{\omega_0^2} (\cos(\omega_0 h) - 1). \tag{3.22}$$

The variances are given by $\tilde{c}_{ii}^h = \nu_d h + \tilde{c}_{ij}^h$.

The bin size dependence of the spike count variance $\tilde{c}_{ii}^h$, covariance $\tilde{c}_{ij}^h$, and correlation coefficient $r_{ij}^h = \tilde{c}_{ij}^h / \tilde{c}_{ii}^h$ determined by equations 3.21 and 3.22 is shown in Figures 2B to 2D for different γ-orders (left column) and oscillation frequencies (right column), respectively. Figure 2A illustrates the corresponding spike train cross-covariance functions 3.13 (left) and 3.20 (right). Note that these cross-covariance functions $\tilde{\psi}_{ij}(\tau)$ reflect the autocovariance functions $\tilde{\psi}_{cc}(\tau)$ of the common sources (see equation 3.6). Only at short timescales the count variances and covariances do not deviate from the Poisson case. In the gamma example (see Figure 2, left), "short" means short compared to the mean interspike interval $1/\nu_c$ of the common source (here, 200 ms). In the Poisson example (see Figure 2, right), the bin size must be considerably smaller than the oscillation period $2\pi/\omega_0$. The count variances $\tilde{c}_{ii}^h$ and covariances $\tilde{c}_{ij}^h$ exhibit a nontrivial dependence on the bin size h. Note that the normalization of the covariance by the variances in the correlation coefficient r_{ij}^h does not remove this dependence. In the gamma example, the deviations from the Poisson case become more pronounced with increasing γ-order and bin size. In the Poisson example, the count variances and covariances oscillate as a function of the bin size.

By comparing the results for the two examples shown in Figure 2 with the case where the common process is a stationary Poisson process, we arrive at the following conclusion. For a given bin size h, spike count variance, covariance, and correlation coefficient are generally decreased if the common process is a gamma process; they are increased if the common process is a Poisson process with sinusoidal rate profile. To gain an intuitive understanding, consider the number of spikes $x^h(t)$ in a certain time window $[t, t+h)$ for a given realization of the point process. In a gamma
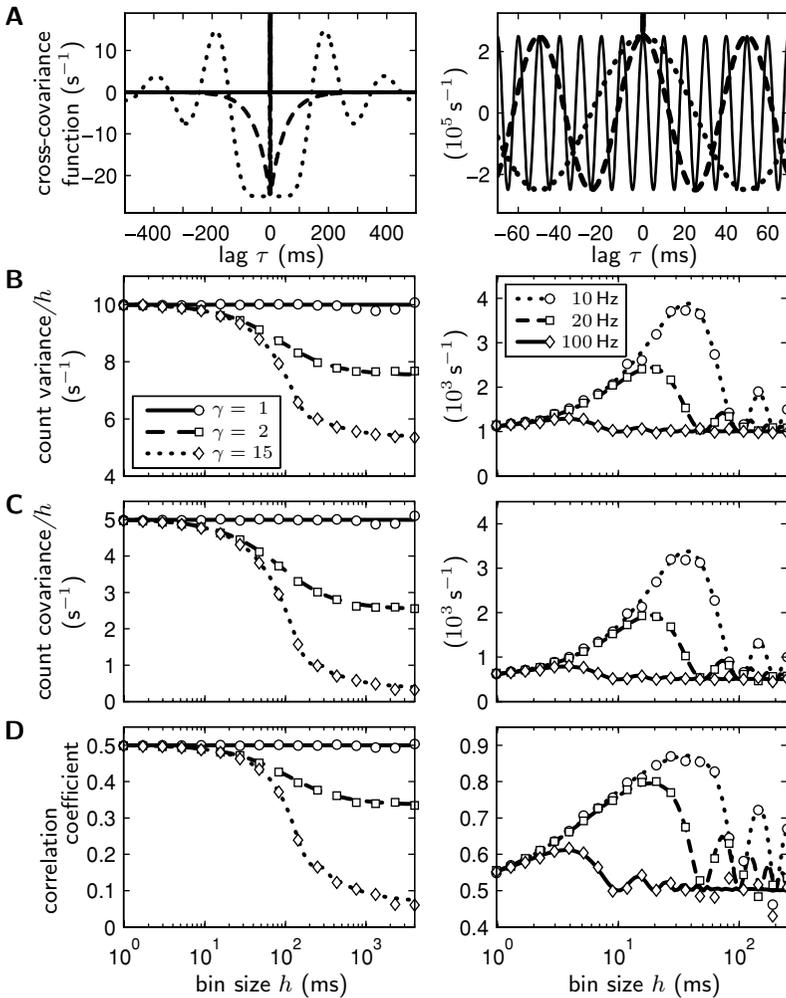
Figure 2: Bin size dependence of spike count correlations (analytical results: curves, simulation: symbols) in the simple common input scenario (see section 3). Left column: common gamma source of orders $\gamma = 1$ (solid, circles), $\gamma = 2$ (dashed, squares), and $\gamma = 15$ (dotted, diamonds) with common input strength $\alpha = 0.5$ and total firing rate $\nu = 10\,\mathrm{s}^{-1}$ (40 trials, simulation time $T = 1000\,\mathrm{s}$). Right column: common Poissonian source with sinusoidal rate function of frequency $f_0 = 10\,\mathrm{Hz}$ (dotted, circles), $f_0 = 20\,\mathrm{Hz}$ (dashed, squares), and $f_0 = 100\,\mathrm{Hz}$ (solid, diamonds; common input strength $\alpha = 0.5$, total firing rate $\nu = 1000\,\mathrm{s}^{-1}$, 10 trials, simulation time $T = 2\,\mathrm{s}$). (A) Spike train cross-covariance functions $\bar{\psi}_{ij}(\tau)$ (zero lag peaks truncated). (B) Normalized spike count variances $\tilde{c}_{ii}^h/h$, (C) covariances $\tilde{c}_{ij}^h/h$, and (D) correlation coefficients r_{ij}^h as function of the bin size h (log-scaled abscissa).

process, the probability of spike generation immediately after a spike is reduced (reflected in the correlation functions shown in Figure 2A, left). Hence, the number of possible spikes in a time window that is small compared to the mean interspike interval is decreased (compared to a stationary Poisson process with the same rate). Conversely, for an oscillatory Poisson process, the spiking probability after spike emission is enhanced for time intervals that are small compared to the oscillation period (see Figure 2A, right). Therefore, the spike count increases. Remember that this does not affect the mean spike count obtained by averaging over realizations of the point process. It does affect, however, the expectation of the square of the spike count and therefore the spike count variance. Studying the variances, we realize that in the common input scenario, each process results from a superposition of a common gamma or inhomogeneous Poisson process, respectively, and a stationary Poissonian background process. In contrast, the spike count covariances reflect the variances of the common process only. Thus, the normalization of the covariance by the variances does not remove the bin size dependence.

A dependence of the count variance $\tilde{c}_{ii}^h$ and the Fano factor $F = \tilde{c}_{ii}^h / v_i h$ (Fano, 1947) on the bin size for (non-Poissonian) renewal processes has already been reported by Rotter, Riehle, Rodriguez Molina, Aertsen, and Nawrot (2005). In particular, the authors point out that the Fano factor of a gamma process is biased toward 1 for small bin sizes. Our considerations demonstrate that this is the case for all point processes with a finite (or zero) interval density $p_1(\tau)$ (interspike interval distribution) at small time lags τ. The autocovariance function (Cox, 1962; Perkel et al., 1967a)

$$\tilde{\psi}_{ii}(\tau) = v_i \left(\delta(\tau) + \sum_{k=1}^{\infty} p_k(|\tau|) \right) - v_i^2$$

of such a process is in the vicinity of $\tau = 0$, always dominated by the delta peak with amplitude v_i. According to equation 2.15, the count variance $\tilde{c}_{ii}^h$ therefore approaches the count mean $v_i h$ for small bin sizes h, resulting in a Fano factor close to one. In other words, at timescales that are small compared to the mean interspike interval, a point process is not distinguishable from a Poisson process.

Figure 2 not only illustrates that measured spike count correlations depend on the choice of the bin size h but also demonstrates that the variance, the covariance, and the correlation coefficient are determined by the statistics of the common source. In the gamma example (left column in Figure 2), the correlation coefficient decreases as the γ-order increases (see Figure 2D, left). This dependence on the γ-order is made explicit in Figure 3A. For common sources with oscillating Poisson statistics (right column in Figure 2), the correlation coefficient decreases with increasing oscillation frequency f_0 (see Figure 2D, right).
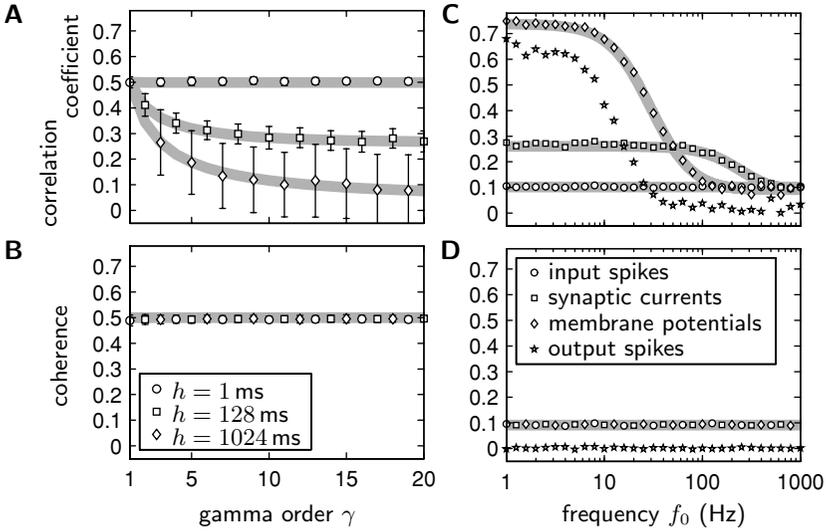
Figure 3: Dependence of common input correlations on the statistics of the presynaptic sources for the simple common input model (left column; see section 3) and the Poisson network model (right column; see model in section 4). Left column (common input model): (A) Measured spike count correlation coefficients r_{ij}^h and (B) averaged high-frequency (>10 Hz) coherences κ for three different bin sizes $h = 1$ ms (circles), $h = 128$ ms (squares), and $h = 1024$ ms (diamonds) as functions of the order γ of the common gamma source (common input strength $\alpha = 0.5$, total firing rate $\nu = 10\,\mathrm{s}^{-1}$). Symbols represent simulation results obtained from averaging over 1000 trials (simulation time per trial $T = 4.096$ s). Error bars indicate standard deviations resulting from 100 repetitions of the experiment each with 10 trials (error bars in A for $h = 1$ ms and in B are too small to be visible). Right column (Poisson network model): (C) Measured spike count correlation coefficients r_{ij} and (D) averaged coherences κ for synaptic input spike counts (circles), synaptic input currents (squares), membrane potentials (diamonds), and output spike counts (stars) as functions of the oscillation frequency f_0 of the presynaptic sources (30 trials, simulation time $T = 1$ s; see section 4.1 for model parameters). Thick gray curves in A and C show analytical results for the correlation coefficient; in B and D, they depict the (effective) common input strengths.

3.4 Coherence. The dependence of the correlation coefficient on the filter properties and on the structure of the spike correlation functions (see Figures 2D and 3A) renders its interpretation difficult and limits its usefulness for the comparison of data from different preparations and laboratories. In section 2.1 we remarked that in contrast to the correlation coefficient, the coherence $\kappa(\omega)$, equation 2.10, is independent of a joint linear filter kernel.
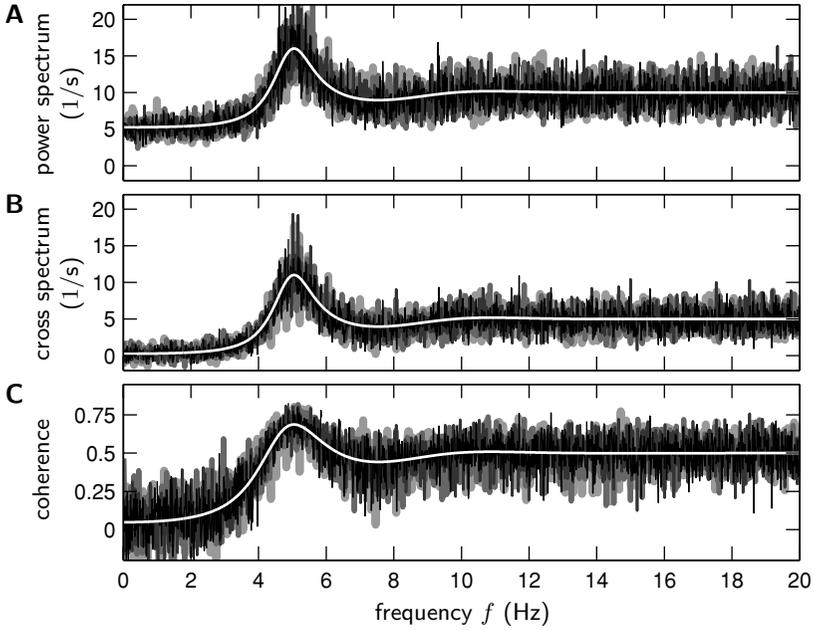
Figure 4: Extraction of correlation from spike trains with structured autocorrelation generated by the simple common input model (see Figure 1A). (A) Spike train power- $\tilde{\Psi}_{ii}(\omega)$ and (B) cross-spectra $\tilde{\Psi}_{ij}(\omega)$ estimated from measured spike count spectra $\tilde{C}_{ii/ij}(\omega)$ (total rate $\nu = 10\,\mathrm{s}^{-1}$, common gamma source with $\gamma = 20$, common input strength $\alpha = 0.5$, simulation time $T = 65.536\,\mathrm{s}$, averaged over 30 trials). The panels show data for four bin sizes superimposed (light gray to black and with decreasing thickness: $h = 0.1, 1, 128,$ and $1024\,\mathrm{ms}$), no further smoothing of graphs. The white curves show analytical results. (C) Coherence $\kappa(\omega) = |\tilde{\Psi}_{ij}(\omega)|/\tilde{\Psi}_{ii}(\omega) = |\tilde{C}_{ij}(\omega)|/\tilde{C}_{ii}(\omega)$.

This is illustrated for the gamma example in Figure 4C. However, the coherence still depends on the shape of the auto- and cross-spectra of the input spike trains. As we assumed mutual independence between the common and the disjoint input processes, equation 3.4, the coherence is given by

$$\kappa(\omega) = \frac{\tilde{\Psi}_{cc}(\omega)}{\tilde{\Psi}_{dd}(\omega) + \tilde{\Psi}_{cc}(\omega)}, \tag{3.23}$$

where $\tilde{\Psi}_{dd}(\omega) := \tilde{\Psi}_{d_i d_i}(\omega) = \tilde{\Psi}_{d_j d_j}(\omega)$. For a large class of point processes the power spectrum becomes constant at high frequencies with its amplitude approaching the numerical value of the firing rate (Jarvis & Mitra, 2001;

Halliday, 2000):

$$\lim_{\omega \to \infty} \tilde{\Psi}_{cc}(\omega) = \nu_c$$
$$\lim_{\omega \to \infty} \tilde{\Psi}_{dd}(\omega) = \nu_d.$$

(3.24)

This is trivial for the disjoint Poissonian processes with $\tilde{\Psi}_{dd}(\omega) = \nu_d$ ($\forall \omega$). But the gamma process also exhibits this property: both the real and the imaginary part of equation 3.12 approach zero in the limit $\omega \to \infty$. With equation 3.11, the first limit in equation 3.24 follows immediately. If the common source is an oscillating Poisson process, its power spectrum, the Fourier transform of equation 3.20, is identical for all frequencies ω except ω_0:

$$\tilde{\Psi}_{cc}(\omega) = \nu_c \qquad (\forall \omega \neq \omega_0).$$

(3.25)

In general, equation 3.24 holds for all point processes with interval densities $p_k(\tau)$ absent of high-frequency components. This becomes apparent by inspection of equation 3.9: if $\mathfrak{F}[p_k(\tau)](\omega) = P_k(\omega)$ vanishes in the limit $\omega \to \infty$ for all orders k, the Fourier transform of the autocorrelation 3.9—the power spectrum—saturates at a constant level determined by the firing rate. Typically natural point processes fulfill this condition. To mention an exception, consider a regular process with a constant interspike interval T: $p_1(\tau) = \delta(\tau - T)$.

Given the property 3.24 and the assumptions of section 3.2 the coherence at high frequencies recaptures the common input strength α:

$$\lim_{\omega \to \infty} \kappa(\omega) = \frac{\nu_c}{\nu_d + \nu_c} = \alpha.$$

(3.26)

Figure 4 compares the power spectra $\tilde{\Psi}_{ii}(\omega) = \tilde{\Psi}_{cc}(\omega) + \tilde{\Psi}_{dd}(\omega)$ (see Figure 4A), the cross-spectra $\tilde{\Psi}_{ij}(\omega) = \tilde{\Psi}_{cc}(\omega)$ (see Figure 4B), and the coherences $\kappa(\omega)$ (see Figure 4C) for the gamma example obtained from simulations with analytical expressions. The spike train spectrum $\tilde{\Psi}_{ii/ij}(\omega)$ based on simulated spike trains is estimated by dividing the spike count spectrum $\tilde{C}_{ii/ij}(\omega)$ by the spectrum $\Phi(\omega)$ of the spike count filter (excluding frequencies with $\Phi(\omega) = 0$). Figure 4 compares results for four different bin sizes. The coherences in Figure 4C are computed directly from the spike count spectra. Both the spectra and the coherence become constant at frequencies above 10 Hz. The total rate $\nu = 10\,\text{s}^{-1}$, the rate $\nu_c = 5\,\text{s}^{-1}$ of the common process, and the common input strength $\alpha = 0.5$ can be clearly identified as the limiting values of the three panels.

Figure 3B summarizes the results for measured high-frequency coherences for different bin sizes h and γ-orders. Here, the coherences are

averaged over frequencies above 10 Hz. In contrast to the correlation co-
efficient (see Figure 3A), the high-frequency coherence depends on neither
the bin size nor the order of the common gamma process.

3.5 Jittered Correlations. In general (see section 2.1), the correlation
coefficient observed for two shot-noise signals results from the interaction
between the correlation functions of the underlying spike trains and the
filters determining the shot noise. In the foregoing, we have considered the
case where the structure of the correlation functions is determined exclu-
sively by the autocorrelations of the presynaptic sources. However, even
in the simplest case where the latter are stationary Poisson processes with
delta-shaped autocorrelations, the resulting cross-correlations can be struc-
tured. If, for example, a presynaptic neuron consistently contributes spikes
to the two input trains with different but static delays, the cross-correlation
exhibits an off-center delta peak. Assuming that joint contributions come
from many different sources and that there is no bias in the distribution of
delays, a temporally extended and centered peak results. The same would
be true for sources that deliver spikes to the two input trains with dynam-
ical delays described by an identical mean delay and nonvanishing uncor-
related temporal jitter. Consider two processes $\xi_i(t)$ and $\xi_j(t)$ constructed
as explained in Figure 1A. Assume that both the common $\xi_c(t)$ and the two
disjoint sources $\xi_{d_{i/j}}(t)$ are homogeneous Poisson processes. If spikes of the
common process $\xi_c(t)$ are precisely copied into both processes $\xi_i(t)$ and $\xi_j(t)$,
the resulting cross-correlation function is delta shaped. However, if one of
the two processes receives a jittered version of the common process,

$$\xi_c^{\text{jit}}(t) = \sum_k \delta(t - t_k + \epsilon_k), \tag{3.27}$$

such that each spike at time t_k is shifted by a random number ϵ_k, the shape of
the cross-covariance function reflects the probability density function (pdf)
$p_{\text{jit}}(\epsilon)$ of ϵ_k:

$$\tilde{\psi}_{ij}(\tau) = \nu_c\, p_{\text{jit}}(\tau). \tag{3.28}$$

Here, ν_c denotes the firing rate of the common source $\xi_c(t)$, which is not
affected by the jittering procedure. Since we assumed that all involved pro-
cesses are Poissonian, the autocovariance functions remain unaffected too:

$$\tilde{\psi}_{ii/jj}(\tau) = \nu\delta(\tau). \tag{3.29}$$

According to equation 2.17, the count correlation coefficient reads

$$r_{ij}^h = \frac{\nu_c}{\nu h} \int_{-h}^{h} \mathrm{d}\tau\, (h - |\tau|) p_{\text{jit}}(\tau). \tag{3.30}$$
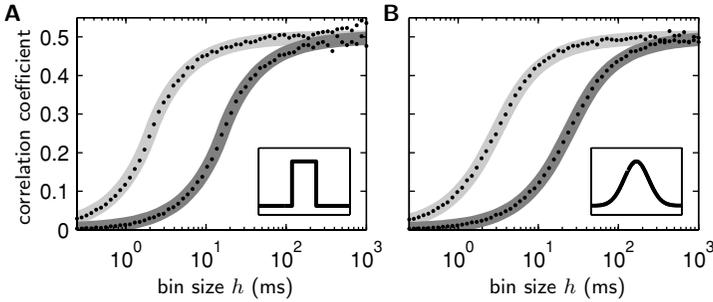
Figure 5: Trivial bin size dependence of the spike count correlation coefficient for temporally extended cross-correlations. Two correlated Poisson spike trains ($\nu = 10\,\text{s}^{-1}$, $\alpha = 0.5$) of duration $T = 1024\,\text{s}$ are constructed as described in Figure 1A. In addition, in one of the spike trains, the spikes from the common source are jittered by a random offset drawn from a symmetric distribution (light gray curves: standard deviation $\sigma = 2\,\text{ms}$; dark gray curves: $\sigma = 16\,\text{ms}$) with zero mean: (A) rectangular and (B) gaussian distribution (see insets). In both panels, the spike count correlation coefficient $\tilde{c}_{ij}/(\nu h)$ is shown (gray curves: analytical results; dots: simulations) as a function of the bin size h (log-scaled abscissa).

Its bin size dependence is illustrated in Figure 5 for a rectangular and a gaussian delay distribution $p_{\text{jit}}(\tau)$ (see appendix B).

With $P_{\text{jit}}(\omega)$ being the Fourier transform of $p_{\text{jit}}(\tau)$, the coherence reads

$$\kappa(\omega) = \frac{\nu_c}{\nu} |P_{\text{jit}}(\omega)|. \tag{3.31}$$

As $p_{\text{jit}}(\tau)$ is a probability density with $P_{\text{jit}}(0) = \int d\tau \, p_{\text{jit}}(\tau) = 1$, the coherence at frequency $\omega = 0$ recaptures the common input strength α:

$$\kappa(0) = \frac{\nu_c}{\nu} = \alpha. \tag{3.32}$$

In contrast to the correlation coefficient, $\kappa(0)$ does not depend on the filter properties. It recaptures the strength of the common input α, however, only if the presynaptic sources are stationary Poisson processes.

In a realistic setting, we must expect that both the spike statistics of the presynaptic sources and the presence of (distributions of) delays will shape the resulting correlation functions. In this case, the coherence in our model reads

$$\kappa(\omega) = \frac{|P_{\text{jit}}(\omega)\tilde{\Psi}_{cc}(\omega)|}{\tilde{\Psi}_{cc}(\omega) + \tilde{\Psi}_{dd}(\omega)}. \tag{3.33}$$
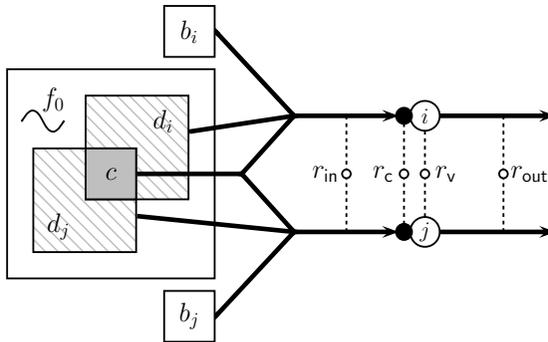
Figure 6: Sketch of the Poisson network model. Neurons i and j receive nonstationary Poissonian inputs from a local network (large box) and independent external sources ($b_{i/j}$). Presynaptic neurons in the local network fire independently with in-phase oscillating firing rates (frequency f_0). Local presynaptic neuron populations (hatched boxes) partially overlap (gray region), thereby decomposing into common (c) and disjoint sources ($d_{i/j}$). The resulting correlations between neurons i and j can be measured between compound input spike trains (r_{in}), total synaptic input currents (r_c), membrane potentials (r_v), and output spike trains (r_{out}).

In section 3.4 we argued that in the neuroscientific context, many processes exhibit power spectra that approach a constant value, the firing rate, in the $\omega \to \infty$ limit. In the absence of temporal jitter, this enables us to determine the common input strength α from the coherence $\kappa(\omega)$ at large frequencies. In the presence of temporal jitter, this approach is problematic if $P_{jit}(\omega)$ decays to zero at large frequencies, which seems natural for non-delta-type jitter distributions. According to equation 3.33, in this case, the high-frequency coherence will become zero too. This is not surprising because if the spread of $p_{jit}(\tau)$ is large, the spike trains become de facto uncorrelated on a short timescale. Hope to recover α rests on the assumption that the temporal spread of $p_{jit}(\tau)$ is much smaller than the timescale of the structure of the autocovariance function $\tilde{\psi}_{cc}(\tau)$, such that $\tilde{\Psi}_{cc}(\omega)$ falls off faster than $P_{jit}(\omega)$.

4 Poisson Model of a Local Cortical Network

4.1 Model Definition. We now turn to the consequences of the filtering of presynaptic spike trains on correlated postsynaptic activity in the light of a simple model that mimics the input statistics in a local cortical network in a volume of about $1\,\text{mm}^3$ (see Figure 6). Rather than describing the activity evolving in a recurrent network (see section 5), we replace at this stage all presynaptic spike trains by (inhomogeneous) Poisson processes but take into account the anatomical and electrophysiological network parameters.

Consider a network of N neurons, a fraction $N_E = \beta N$ being excitatory and the rest $N_I = (1 - \beta)N$ inhibitory. Each neuron receives a fixed number of $K = \alpha N$ synapses from the local network. $K_E = \beta K$ of them are excitatory and $K_I = (1 - \beta)K$ inhibitory. In addition to these local inputs, every neuron is driven by an excitatory external Poissonian source. The total input of neuron i ($i \in [1, N]$) thus reads

$$x_{q,i}(t) = \sum_{k=1}^{N} (\xi_k * f_{q,ik})(t) + (\xi_{i,\text{ext}} * f_{q,i,\text{ext}})(t). \tag{4.1}$$

Here, $\xi_k(t)$ denotes the spike train of a presynaptic neuron k and $\xi_{i,\text{ext}}(t)$ the external Poissonian process arriving at neuron i. The (linear) filter kernels $f_{q,ik}(t)$ and $f_{q,i,\text{ext}}(t)$ describe the responses of the postsynaptic neuron i on the different presynaptic spike trains $\xi_k(t)$ and $\xi_{i,\text{ext}}(t)$ at different signal levels $q \in \{\text{in, c, v}\}$ (see below).

For simplicity, we assume that spikes arriving at excitatory or inhibitory synapses cause responses (postsynaptic currents or postsynaptic potentials) that differ only in sign and amplitude, not in shape. We may thus simplify our notation and write

$$f_{q,ik}(t) = \begin{cases} f_q(t) & \text{if synapse } k \to i \text{ is excitatory} \\ -g f_q(t) & \text{if synapse } k \to i \text{ is inhibitory} \\ 0 & \text{if synapse } k \to i \text{ does not exist} \end{cases} \tag{4.2}$$

and $f_{q,i,\text{ext}} = f_q(t)$ ($\forall i$). The parameter g denotes the relative strength of inhibition.

For demonstration we discuss the synaptic input, equation 4.1, at three different signal levels: the weighted input spike count $x_{\text{in},i}(t)$, the total synaptic input current $x_{c,i}(t)$, and the free membrane potential $x_{v,i}(t)$. For the input spike count $x_{\text{in},i}(t)$, we use the spike count kernel $f_{\text{in}}(t)$ as defined in equation 2.14 with a bin size h. The synaptic input current $x_{c,i}(t)$ is obtained by convolving the presynaptic spike trains with an α-function,

$$f_c(t) = \begin{cases} 0 & t < 0 \\ J e \tau_s^{-1} t e^{-t/\tau_s} & t \geq 0 \end{cases}, \tag{4.3}$$

with a postsynaptic current (PSC) amplitude J and a time constant τ_s. The free membrane potential $x_{v,i}(t)$ is derived from the synaptic current by low-pass filtering with an exponential kernel:

$$\tilde{f}_v(t) = \begin{cases} 0 & t < 0 \\ C_m^{-1} e^{-t/\tau_m} & t \geq 0 \end{cases}. \tag{4.4}$$

Here, τ_m denotes the membrane time constant and C_m the membrane capacitance. The full membrane potential kernel (the postsynaptic potential, PSP) results from the convolution of $f_c(t)$ and $\tilde{f}_v(t)$:

$$f_v(t) = \frac{J e}{C_m \tau_s} \left(\frac{1}{\tau_s} - \frac{1}{\tau_m} \right)^{-2} \left[\left(\frac{1}{\tau_m} - \frac{1}{\tau_s} \right) t e^{-t/\tau_s} - e^{-t/\tau_s} + e^{-t/\tau_m} \right].$$

(4.5)

Since all four signal types are treated as shot noise, their marginal and joint statistics can be described analytically if the statistics of the input spike trains are known (see section 2.1). In addition, we numerically study the output $x_{out,i}(t)$ of our model neurons, which is defined by a Heaviside function of the free membrane potential:

$$x_{out,i}(t) = \Theta(x_{v,i}(t) - \theta) = \begin{cases} 1 & x_{v,i}(t) \geq \theta \\ 0 & \text{else} \end{cases}.$$

(4.6)

Although this simple static nonlinearity results in a (piecewise) continuous binary output, we refer to it as "spiking" activity.

To simplify the derivation of the input correlation functions and spectra in section 4.2 we assume that the network is homogeneous in the sense that all local firing rates and auto- and cross-covariance functions are identical:

$$\begin{aligned} \nu(t) &:= \nu_k(t) = \mathrm{E}\left[\xi_k(t)\right] & (\forall k), \\ \tilde{\psi}_a(\tau) &:= \tilde{\psi}_{kk}(\tau) = \mathrm{E}\left[\tilde{\xi}_k(t)\tilde{\xi}_k(t+\tau)\right] & (\forall k), \\ \tilde{\psi}_c(\tau) &:= \tilde{\psi}_{kl}(\tau) = \mathrm{E}\left[\tilde{\xi}_k(t)\tilde{\xi}_l(t+\tau)\right] & (\forall k \neq l). \end{aligned}$$

(4.7)

The external sources are treated as stationary Poisson processes with rate $\mathrm{E}\left[\xi_{i,ext}(t)\right] = \beta K \nu_{ext}$ and autocovariance function

$$\tilde{\psi}_{ext}(\tau) := \mathrm{E}\left[\tilde{\xi}_{i,ext}(t)\tilde{\xi}_{i,ext}(t+\tau)\right] = \beta K \nu_{ext} \delta(\tau) \quad (\forall i).$$

(4.8)

Assume further that the correlations between the external sources of different target cells i and j and those between external processes $\xi_{i,ext}(t)$ and local spike trains $\xi_k(t)$ can be neglected. Local spike trains are described as Poisson processes with time-dependent rate function $\nu(t)$. Similar to section 3.2.2 we consider a situation where the firing rates of all local neurons covary for a given trial (or network realization). Across trials, however, the rate functions are nonstationary, such that the trial-averaged firing rate $\nu := \mathrm{E}\left[\nu(t)\right]$ is constant. If we assume that there are no correlations among the local spike trains beyond those arising from covarying firing rates, the

local covariance functions read

$$\tilde{\psi}_a(\tau) = \nu\delta(\tau) + \tilde{\gamma}(\tau)$$
$$\tilde{\psi}_c(\tau) = \tilde{\gamma}(\tau). \tag{4.9}$$

Here, $\tilde{\gamma}(\tau)$ denotes the rate covariance function (see section 3.2.2):

$$\tilde{\gamma}(\tau) := \mathrm{E}\left[\nu(t)\nu(t+\tau)\right] - \nu^2. \tag{4.10}$$

As an example, we focus on sinusoidal rate functions

$$\nu(t) = \nu\left[1 + \cos(\omega_0 t + \phi)\right], \tag{4.11}$$

with a fixed oscillation frequency $f_0 = \omega_0/2\pi$. As in section 3.2.2, we draw the phases for each trial randomly from a uniform distribution ($\phi \in [0, 2\pi)$). The rate covariance function thus becomes

$$\tilde{\gamma}(\tau) = \frac{1}{2}\nu^2\cos(\omega_0\tau). \tag{4.12}$$

Oscillatory population activity has been reported both experimentally (Eckhorn et al., 1988; Singer et al., 1988; Aertsen & Arndt, 1993; Gray, 1994; Fries et al., 2001) and theoretically (van Vreeswijk, Abbott, & Ermentrout, 1994; Brunel & Hakim, 1999; Brunel, 2000; see the companion article in this issue: B. Kriener, T. Tetzlaff, A. Aertsen, M. Diesmann, & S. Rotter, "Correlations and Population Dynamics in Cortical Networks") as a prominent feature of local cortical networks. With the help of the Poisson network model described here, we investigate how common-input correlations r_{in}, r_c, r_v, and r_{out} at the different signal levels (weighted input spike counts [in], synaptic currents [c], free membrane potentials [v] and output spikes [out]) are affected by the presence and the frequency f_0 of these oscillations (see Figure 6).

If not stated otherwise, we use the following set of parameters: $\alpha = 0.1$ (network connectivity), $K = 1250$ (number of synapses per neuron), $\beta = 0.8$ (relative number of excitatory cells), $g = 6$ (relative strength of inhibition), $\nu = 10\,\mathrm{s}^{-1}$ (local single neuron firing rate), $\nu_{\mathrm{ext}} = 8.8\,\mathrm{s}^{-1}$ (firing rate of external sources), $h = 0.1\,\mathrm{ms}$ (bin size of input count signals), $J = 50\,\mathrm{pA}$ (PSC amplitude), $\tau_{\mathrm{s}} = 0.5\,\mathrm{ms}$ (synaptic time constant), $\tau_{\mathrm{m}} = 10\,\mathrm{ms}$ (membrane time constant), $C_{\mathrm{m}} = 250\,\mathrm{pF}$ (membrane capacitance), and $\theta = 20\,\mathrm{mV}$ (spike threshold). With the chosen values for J, τ_{s}, τ_{m}, and C_{m} we obtain a PSP amplitude of $0.22\,\mathrm{mV}$ (for excitatory synapses) and a PSP rise time to the maximum of $2.2\,\mathrm{ms}$ (see equation 4.5). The same parameters are used for the network model in section 5.

4.2 Correlation Functions. With equations 2.4 and 4.1 and the assumption that the external sources are mutually uncorrelated, the covariance functions of the two shot-noise processes $x_i(t)$ and $x_j(t)$ are given by

$$\tilde{c}_{ij}(\tau) = \sum_{k=1}^{N} \left(\tilde{\psi}_{kk} * \phi_{ik}^{jk} \right)(\tau) + \sum_{k=1}^{N} \sum_{l \neq k}^{N} \left(\tilde{\psi}_{kl} * \phi_{ik}^{jl} \right)(\tau)$$

$$+ \delta_{ij} (\tilde{\psi}_{\text{ext}} * \phi_{\text{ext}})(\tau). \tag{4.13}$$

Here, $\phi_{ik}^{jl}(\tau)$ denotes the cross-correlation between the filter kernels $f_{ik}(\tau)$ and $f_{jl}(\tau)$, $\phi_{\text{ext}}(\tau)$ the autocorrelation of $f_{i,\text{ext}}(t)$. The Kronecker symbol δ_{ij} is one for $i = j$ and zero otherwise. In the frequency domain, equation 4.13 reads

$$\tilde{C}_{ij}(\omega) = \sum_{k=1}^{N} \tilde{\Psi}_{kk}(\omega) \Phi_{ik}^{jk}(\omega) + \sum_{k=1}^{N} \sum_{l \neq k}^{N} \tilde{\Psi}_{kl}(\omega) \Phi_{ik}^{jl}(\omega) + \delta_{ij} \tilde{\Psi}_{\text{ext}}(\omega) \Phi_{\text{ext}}(\omega).$$

$$\tag{4.14}$$

With the homogeneity assumption 4.7, the spike train power- and cross-spectra become independent of the presynaptic neuron indices:

$$\tilde{C}_{ij}(\omega) = \tilde{\Psi}_a(\omega) \sum_{k=1}^{N} \Phi_{ik}^{jk}(\omega) + \tilde{\Psi}_c(\omega) \sum_{k=1}^{N} \sum_{l \neq k}^{N} \Phi_{ik}^{jl}(\omega) + \delta_{ij} \tilde{\Psi}_{\text{ext}}(\omega) \Phi_{\text{ext}}(\omega).$$

$$\tag{4.15}$$

As excitatory and inhibitory synapses differ only in amplitude, but not in their kinetics (see equation 4.2), the power spectrum of $x_i(t)$ reads

$$\tilde{C}_{ii}(\omega) = \Phi(\omega) \cdot \{ \tilde{\Psi}_a(\omega)(K_E + g^2 K_I) + \tilde{\Psi}_c(\omega)(K_E[K_E - 1]$$

$$+ g^2 K_I[K_I - 1] - 2g K_E K_I) + \tilde{\Psi}_{\text{ext}}(\omega) \}. \tag{4.16}$$

Here, $\Phi(\omega)$ denotes the power spectrum of the (excitatory) filter kernel $f(t)$. Assuming that the numbers of excitatory and inhibitory synapses are large (i.e., $K_E \gg 1$ and $K_I \gg 1$), we finally obtain

$$\tilde{C}_{ii}(\omega) = \Phi(\omega) \{ (K_E + g^2 K_I) \tilde{\Psi}_a(\omega) + (K_E - g K_I)^2 \tilde{\Psi}_c(\omega) + \tilde{\Psi}_{\text{ext}}(\omega) \}$$

$$= \Phi(\omega) \{ K(\beta + g^2[1 - \beta]) \tilde{\Psi}_a(\omega) + K^2(\beta - g[1 - \beta])^2 \tilde{\Psi}_c(\omega)$$

$$+ \tilde{\Psi}_{\text{ext}}(\omega) \}. \tag{4.17}$$

For the cross-spectrum $\tilde{C}_{ij}(\omega)$ ($i \neq j$), the first term $\sum_{k=1}^{N} \Phi_{ik}^{jk}(\omega)$ in equation 4.15 represents the overlap between the presynaptic neuron populations of the two postsynaptic target cells i and j. Given a random network of size N and a connection probability α, the average size of this overlap is $C = \alpha^2 N$. The fraction $C_E = \beta C$ thereof represents the number of common excitatory presynaptic cells and $C_I = (1 - \beta)C$ the number of shared inhibitory sources. The cross-spectrum ($i \neq j$) thus reads

$$\tilde{C}_{ij}(\omega) = \Phi(\omega)\{(C_E + g^2 C_I)\tilde{\Psi}_a(\omega) + (K_E - g K_I)^2 \tilde{\Psi}_c(\omega)\}$$
$$= \Phi(\omega)\{\alpha K(\beta + g^2[1 - \beta])\tilde{\Psi}_a(\omega) + K^2(\beta - g[1 - \beta])^2 \tilde{\Psi}_c(\omega)\}. \tag{4.18}$$

Note that apart from the spectrum $\tilde{\Psi}_{\text{ext}}(\omega)$ of the external source, the cross-spectra and power spectra differ only in the factor α, the network connectivity.

With the Fourier transforms of equations 4.8, 4.9, and 4.12,

$$\tilde{\Psi}_a(\omega) = \nu + \frac{1}{2}\nu^2\pi\left(\delta[\omega - \omega_0] + \delta[\omega + \omega_0]\right)$$

$$\tilde{\Psi}_c(\omega) = \frac{1}{2}\nu^2\pi\left(\delta[\omega - \omega_0] + \delta[\omega + \omega_0]\right) \tag{4.19}$$

$$\tilde{\Psi}_{\text{ext}}(\omega) = \beta K \nu_{\text{ext}},$$

the shot-noise spectra, equations 4.17 and 4.18, further simplify to

$$\tilde{C}_{ii}(\omega) = a_{ii}\Phi(\omega) + \pi b \Phi(\omega)\left(\delta[\omega - \omega_0] + \delta[\omega + \omega_0]\right)$$
$$\tilde{C}_{ij}(\omega) = a_{ij}\Phi(\omega) + \pi b \Phi(\omega)\left(\delta[\omega - \omega_0] + \delta[\omega + \omega_0]\right). \tag{4.20}$$

The prefactors a_{ii}, a_{ij}, and b are given by

$$a_{ii} = K\nu(\beta + g^2[1 - \beta]) + K\beta\nu_{\text{ext}}$$

$$a_{ij} = \alpha K\nu(\beta + g^2[1 - \beta]) \tag{4.21}$$

$$b = \frac{1}{2}K\nu^2(\alpha[\beta + g^2(1 - \beta)] + [\beta - g(1 - \beta)]^2).$$

The inverse Fourier transform of equation 4.20 yields the shot-noise covariance functions

$$\tilde{c}_{ii}(\tau) = a_{ii}\phi(\tau) + b\Phi(\omega_0)\cos(\omega_0\tau)$$
$$\tilde{c}_{ij}(\tau) = a_{ij}\phi(\tau) + b\Phi(\omega_0)\cos(\omega_0\tau). \tag{4.22}$$
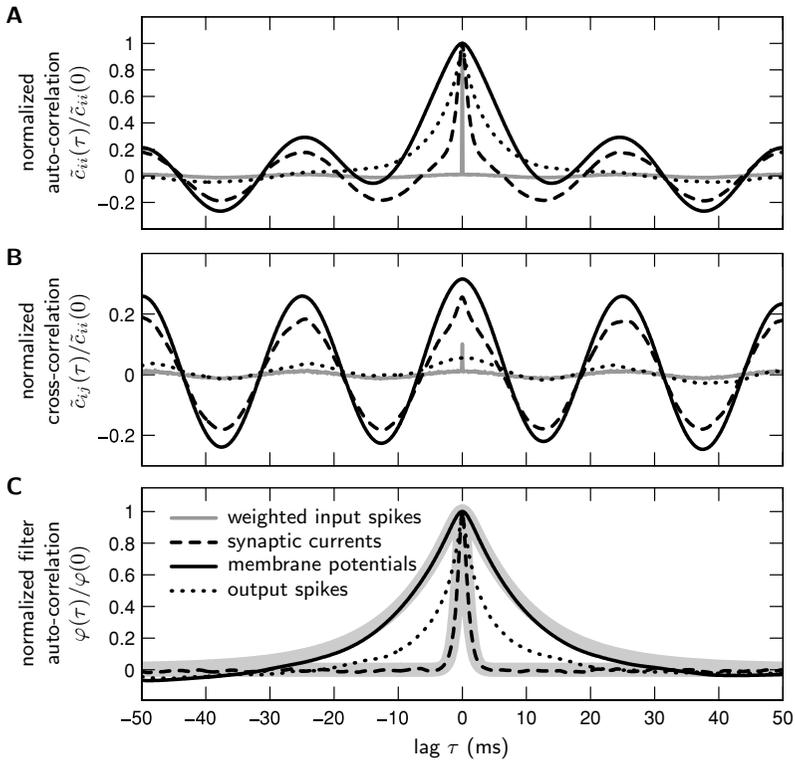
Figure 7: Reconstruction of filter autocorrelations for the Poisson network model shown in Figure 6. Normalized autocovariance functions $\tilde{c}_{ii}(\tau)/\tilde{c}_{ii}(0)$ (A) and cross-covariance functions $\tilde{c}_{ij}(\tau)/\tilde{c}_{ii}(0)$ (B) for input spike counts (solid gray line), synaptic currents (dashed line), membrane potentials (solid black line), and output spike counts (dotted line). Presynaptic neuron populations oscillate with $f_0 = 40$ Hz (simulation time $T = 1$ s, 50 trials). (C) Normalized filter autocorrelations $\phi(\tau)/\phi(0)$ of synaptic input currents, membrane potentials, and output spike counts obtained from the differences $\tilde{c}_{ii}(\tau) - \tilde{c}_{ij}(\tau)$ between the corresponding auto- and cross-covariance functions shown in A and B. Thick gray curves depict autocorrelations of the kernels for synaptic currents and membrane potentials used in the simulations. See section 4.1 for model parameters.

4.3 Autocorrelation and Filter Dependence of Correlations. Figure 7 shows the normalized auto- and cross-covariance functions $\tilde{c}_{ii}(\tau)/\tilde{c}_{ii}(0)$ and $\tilde{c}_{ij}(\tau)/\tilde{c}_{ii}(0)$ (see Figures 7A and 7B, respectively) obtained from simulations with an oscillation frequency $f_0 = 40$ Hz. The covariance functions for the weighted input spike counts, measured at a fine scale of $h = 0.1$ ms, are dominated by the delta peaks at $\tau = 0$. Due to the filtering at the synapses

and by the membrane, these peaks are more and more flattened, thereby emphasizing the oscillatory structure of the (normalized) covariance functions. Note that the correlation coefficients, that is, the zero-lag values of the normalized cross-covariance functions in Figure 7B, are increased by the filtering procedure. The dotted curves in Figure 7 represent the measured covariance functions of the output "spike" signals. The threshold mechanism modeling the spike dynamics obviously causes a decrease of the correlation coefficient. At the same time, the peaks of the covariance functions around $\tau = 0$ are slightly sharpened compared to the membrane potential level. Still, the peaks have a considerable width of several milliseconds, although the correlation functions of the unfiltered input signals are sharp (gray curve in Figure 7B). Thus, the structure of the correlation function of the output spike train is at least partially determined by the neuronal filter properties. Changes in synaptic or membrane time constants, for example, therefore provide a possible explanation for experimentally observed changes in correlation strengths or timescales (Aertsen et al., 1989; Vaadia et al., 1995; Kohn & Smith, 2005; Sakurai & Takahashi, 2006).

The variance $(i = j)$ and covariance of the filtered signals are obtained by evaluating equation 4.22 at $\tau = 0$:

$$\tilde{c}_{ij} = a_{ij}\phi(0) + b\Phi(\omega_0). \tag{4.23}$$

The dependence of the correlation coefficient $r_{ij} = \tilde{c}_{ij}/\tilde{c}_{ii}$ on the oscillation frequency $f_0 = \omega_0/2\pi$ is shown in Figure 3C for the four different signal levels: $x_{\text{in},i/j}(t)$, $x_{\text{c},i/j}(t)$, $x_{\text{v},i/j}(t)$, and $x_{\text{out},i/j}(t)$. Only correlations between the weakly filtered input signals $x_{\text{in},i/j}(t)$ are apparently unaffected by the oscillation frequency f_0 in the interval [1,1000] Hz. Low-pass filtering by the synapses and membranes results in a clear frequency dependence of the correlation coefficient. Note that the frequency dependence of the output correlations is governed by the membrane potential correlations. In other words, a population of neurons is sensitive to changes in the input correlation and reacts accordingly. Thus, spike synchrony in neural networks can be effectively modulated by the frequency of network oscillations and the filter properties of the neurons, that is, the time constants of the synapses and the membranes. Both mechanisms are physiologically relevant: membrane time constant, for example, can change as a result of changes in membrane conductances (Destexhe & Paré, 1999; Destexhe, Rudolph, & Pare, 2003; Kuhn, Aertsen, & Rotter, 2004). Network oscillations at various frequency bands are reported both experimentally and theoretically and are known to occur in relation to the experimental protocol (Eckhorn et al., 1988; Singer et al., 1988; Aertsen & Arndt, 1993; Gray, 1994; Fries et al., 2001; van Vreeswijk et al., 1994; Brunel & Hakim, 1999; Brunel, 2000; Kriener et al., this issue).

Under certain circumstances, the dependence of the correlation coefficient on the filter characteristics and the autocorrelation structure of

the presynaptic sources disappears. If we neglected the external sources, $\tilde{\psi}_{\text{ext}}(\tau) = 0$, and assume that the spike trains in the network are uncorrelated, $\tilde{\psi}_c(\tau) = 0$, the shot-noise covariance functions (Fourier transforms of equations 4.17 and 4.18) become

$$
\begin{aligned}
\tilde{c}_{ij}(\tau) &= \alpha K (\beta + g^2[1 - \beta])(\tilde{\psi}_a * \phi)(\tau) \\
&= \alpha \tilde{c}_{ii}(\tau).
\end{aligned}
\tag{4.24}
$$

In this case, the correlation coefficient,

$$
r_{ij} = \frac{\tilde{c}_{ij}(0)}{\sqrt{\tilde{c}_{ii}(0)\tilde{c}_{jj}(0)}} = \alpha,
\tag{4.25}
$$

is constant and equals the network connectivity α, regardless of the presynaptic autocovariance function $\tilde{\psi}_a(\tau)$ and the filter autocorrelation $\phi(\tau)$.

4.4 Coherence. In section 3.4 we showed that for the simple common input model, the common input strength α can be recaptured from the high-frequency input coherence for a large class of spike processes. In the network model discussed here, α expresses the network connectivity (see section 4.1). We now demonstrate that the input coherence can provide an estimation for α also in this extended model, which incorporates excitatory and inhibitory local inputs, external sources, and correlated spiking caused by covarying firing rates.

Through inspection of equations 4.17 and 4.18, it becomes clear that the coherence $\kappa(\omega) = |\tilde{C}_{ij}(\omega)|/\tilde{C}_{ii}(\omega)$ generally depends on both the marginal ($\tilde{\Psi}_a(\omega)$) and the joint statistics ($\tilde{\Psi}_c(\omega)$) of the presynaptic spike trains. In the high-frequency limit, the coherence reads

$$
\lim_{\omega \to \infty} \kappa(\omega) = \frac{\alpha(\beta + g^2[1 - \beta]) + r K (\beta - g[1 - \beta])^2}{(\beta + g^2[1 - \beta]) + r K (\beta - g[1 - \beta])^2 + \beta \frac{v_{\text{ext}}}{v}}.
\tag{4.26}
$$

Here, r denotes the spike train correlation coefficient (see appendix A). Only if $r = 0$ and $v_{\text{ext}} = 0$, the high-frequency coherence recaptures the connectivity α.

In our specific example, where spike correlations result from oscillating covarying firing rates, the connectivity α can still be estimated from the coherences at frequencies $\omega \neq \pm\omega_0$. Here, we obtain, with equations 4.20 and 4.21,

$$
\kappa(\omega)|_{\omega \neq \pm\omega_0} = \frac{a_{ij}}{a_{ii}} = \alpha \left[1 + \frac{v_{\text{ext}}}{v} \frac{\beta}{\beta + g^2(1 - \beta)} \right]^{-1}.
\tag{4.27}
$$

The correct network connectivity α is retrieved only if the rate ν_{ext} of the external input is zero. This is intuitively clear since both the external and the local disjoint inputs contribute to the uncorrelated parts of the input signals and are indistinguishable at this level. The actual common input strength—the ratio between common and total inputs—is lowered by the external sources. Nevertheless, $\kappa(\omega)$ evaluated at $\omega \neq \pm\omega_0$ provides a good measure of the network connectivity α if the local input fluctuations are larger than those from the external sources. In our network model, this is indeed the case, mostly due to the fact that (local) inhibitory inputs have a much stronger impact than excitatory (local and external) ones. For our choice of parameters ($\nu \approx \nu_{\text{ext}}$, $\beta = 0.8$, $g = 6$), the correction term in equation 4.27 is close to one ($\approx 10/11$). Figure 3D shows coherences measured in simulations (symbols) and obtained from equation 4.27 (gray line). The simulation results represent coherences averaged over all frequencies $f \in [0, 1000]$ Hz except f_0. The coherences for all input signals ($x_{\text{in},i/j}(t)$, $x_{\text{c},i/j}(t)$, $x_{\text{v},i/j}(t)$) are close to $\alpha = 0.1$. They depend on neither the filter characteristics nor the network oscillation frequency f_0. Also, the measured output coherences for $x_{\text{out},i/j}(t)$ do not depend on f_0. They are, however, much smaller than α (of the order of 10^{-3}). Obviously correlations (coherences) between input signals (synaptic currents, membrane potentials) provide much more information about the underlying network structure than correlations between spike signals.

4.5 Filter Reconstruction. In the Poisson network model, common-input correlations affect only the amplitude a_{ij} of the shot-noise cross-covariance function in equation 4.22. The difference between the auto- and cross-covariance functions of the filtered input signals,

$$\tilde{c}_{ii}(\tau) - \tilde{c}_{ij}(\tau) = (a_{ii} - a_{ij})\phi(\tau), \tag{4.28}$$

thus reveals the filter autocorrelation $\phi(\tau)$ up to the prefactor $a_{ii} - a_{ij}$ (which is generally unknown). Consequently, basic features of the filter kernel $f(t)$ can be reconstructed from the covariance functions $\tilde{c}_{ii}(\tau)$ and $\tilde{c}_{ij}(\tau)$ of two simultaneously recorded shot-noise signals $x_{i/j}(t)$; prior knowledge about the unfiltered input signals (i.e., the underlying spike trains) is not required. This is illustrated in Figure 7 for correlation functions measured at different signal levels in simulations of the Poisson network model with rate functions oscillating at $f_0 = 40$ Hz. As shown in Figure 7C, the normalized autocorrelations $\phi(\tau)$ of the PSC and PSP kernels are well recaptured by the difference between measured auto- and cross-covariance functions. The time constants of the synaptic currents ($\tau_s = 0.5$ ms) and membrane potentials ($\tau_m = 10$ ms) can be estimated from the decay times of these curves.

The procedure described here is strictly valid only if the input spike trains exhibit (inhomogeneous) Poissonian statistics. Nevertheless, in section 5.2

we show that synaptic and membrane time constants can be correctly determined by the same method also in networks of integrate-and-fire (I&F) neurons with non-Poissonian firing statistics.

5 Balanced Recurrent I&F Network

5.1 Model Definition. In section 4 we modeled the spike trains in a random network as (inhomogeneous) Poisson processes and studied the responses of isolated cells without considering their feedback on the whole system. In this section, we describe a randomly connected network of excitatory and inhibitory integrate-and-fire neurons (as described in Brunel, 2000). The synaptic input current $x_{c,i}(t)$ of neuron i is described similarly to section 4 by equations 4.1 to 4.3 with the same parameters $J = 50\,\text{pA}$ and $\tau_s = 0.5\,\text{ms}$. The relative strength of inhibition is set to $g = 6$ here. The subthreshold membrane potential dynamics is governed by

$$\tau_m \dot{v}_i = -v_i(t) + R x_{c,i}(t - D), \tag{5.1}$$

with a membrane time constant $\tau_m = 10\,\text{ms}$, a membrane capacitance $C_m = \tau_m/R = 250\,\text{pF}$ (corresponding to a membrane resistance $R = 40\,\text{M}\Omega$), and a fixed spike transmission delay $D = 2\,\text{ms}$. With the chosen values for J, τ_s, τ_m, and C_m, each arriving excitatory spike causes a membrane depolarization of 0.22 mV amplitude with a rise time to the maximum of 2.2 ms. If the membrane potential $v_i(t_k)$ reaches the threshold $\theta = 20\,\text{mV}$, a spike is emitted at time t_k. After spike emission, the membrane is reset and clamped to zero for an absolute refractory period $\tau_{\text{ref}} = 2\,\text{ms}$.

The network architecture is similar to that in section 4. The fraction of excitatory neurons $\beta = N_E/N$ is set to 0.8, the total number of synapses per neuron to $K = 1250$. Thus, each neuron receives $K_E = \beta K = 1000$ excitatory and $K_I = (1 - \beta)K = 250$ inhibitory inputs randomly drawn from the local network. We study the effect of the network connectivity $\alpha = K/N = K_E/N_E = K_I/N_I$ on correlation measures like the correlation coefficient or the coherence by varying the network size N ($N = 12{,}500, 6250, 3125$ corresponding to $\alpha = 0.1, 0.2,$ and 0.4). In addition to the local inputs, each neuron is excited by $K_{\text{ext}} = 1000$ external afferents, which are modeled as independent stationary Poissonian processes of rate $\nu_{\text{ext}} \approx 8.8\,\text{s}^{-1}$.

We simulated networks of three different connectivities ($\alpha = 0.1, 0.2,$ 0.4) with a temporal resolution of 0.1 ms for 10 s. To suppress onset effects, the initial membrane potentials were normally distributed with a mean of 10 mV and a standard deviation of 4 mV. For data analysis, we recorded synaptic input currents from 10 and spikes from 2000 randomly chosen neurons. Free membrane potentials were obtained by low-pass filtering of the synaptic currents according to equation 5.1. In accordance with the study of Brunel (2000), we found individual neurons firing irregularly at low rates of about $9\,\text{s}^{-1}$, independent of the connectivity α.

5.2 Filter Reconstruction. In section 4.5 we argued that the auto- and cross-correlation functions of the linearly filtered signals contain valuable information about the shape of the filter kernel. In a network of Poisson neurons, the filter autocorrelation $\phi(\tau)$ can be reconstructed from the difference between the shot-noise auto- and cross-covariance functions. However, the I&F neurons, clearly do not fire with Poissonian statistics. The population-averaged autocorrelation (see the inset in Figure 8A) exhibits a trough around the central peak indicating decreased firing probability immediately after or before spike emission (refractoriness). Also the power spectra (see Figure 9C) are not completely flat. Still, as illustrated in Figure 8C, the shapes of the PSC and PSP autocorrelations are nicely recaptured by the difference between the auto- and cross-covariance functions of the synaptic input currents and membrane potentials shown in Figures 8A and 8B.

In contrast to the results obtained for synaptic input currents and membrane voltages, correlations between output spike trains (see the dotted curve in Figure 8B, spike count signals, bin size 0.1 ms) are extremely weak.

5.3 Estimation of Network Connectivity from Measured Correlations. In sections 3 and 4, we demonstrated that input coherences at high frequencies provide a reliable measure of the common input strength. In the Poisson network model (see section 4), we showed that the common-input strength reflects the connectivity $\alpha = K/N$ in a random network. Here, we investigate whether the high-frequency input coherences can be used as a tool to estimate the network connectivity in a network of integrate-and-fire neurons.

The top three panels of Figure 9 show for three different network connectivities $\alpha = 0.1$, 0.2, and 0.4 the population averaged power spectra $E_i[\tilde{C}_{ii}(\omega)]$ of the total synaptic input currents (see Figure 9A) and free membrane potentials (see Figure 9B), and the power spectra $E_i[\tilde{\Psi}_{ii}(\omega)] \approx E_i[\tilde{C}_{ii}(\omega)]/h^2$ of the output spike trains (see Figure 9C), estimated from their spike count signals (bin size 0.1 ms). The spectra at all three signal levels show no essential differences for the different connectivities. Those for synaptic currents and membrane potentials are dominated by the low-pass characteristics of the individual synapses and membranes, respectively. The power spectra of the output spike trains are characterized by the white spectrum of a Poisson process with an additional dead time (Gerstner & Kistler, 2002). As mentioned in section 3.4, the spike train power at high frequencies equals the average firing rate (here $9.4\,\text{s}^{-1}$, $9.2\,\text{s}^{-1}$, and $9.5\,\text{s}^{-1}$ for $\alpha = 0.1$, 0.2, and 0.4, respectively).

Figures 9D, 9E, and 9F show the corresponding population averaged coherences $|E_{ij}[\tilde{C}_{ij}(\omega)]|/E_i[\tilde{C}_{ii}(\omega)]$. Clearly, higher connectivities result in higher coherences at all frequencies. All coherences exhibit a broad peak in the range 30 Hz to 100 Hz and less dominant peaks at higher frequencies. These oscillatory components are related to the membrane time constants of the individual neurons and the spike transmission delays (e.g., Brunel,
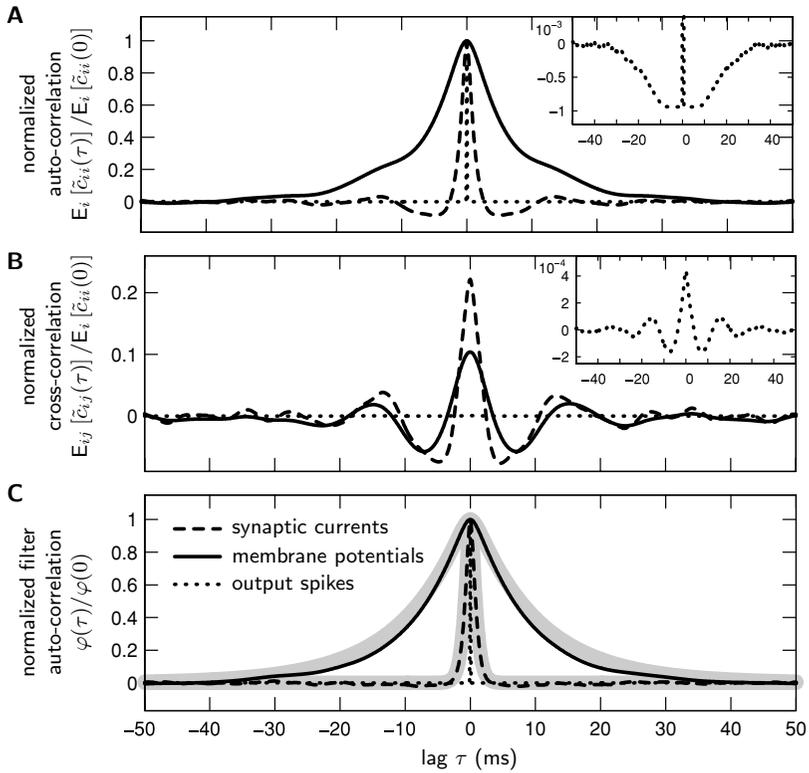
Figure 8: Reconstruction of filter autocorrelations from I&F network simulations for a network connectivity $\alpha = 0.1$. Population-averaged normalized autocovariance functions $E_i \left[\tilde{c}_{ii}(\tau) \right] / E_i \left[\tilde{c}_{ii}(0) \right]$ (A) and cross-covariance functions $E_{ij} \left[\tilde{c}_{ij}(\tau) \right] / E_i \left[\tilde{c}_{ii}(0) \right]$ (B) for synaptic currents (dashed line), membrane potentials (solid black line) and output spike counts (dotted line). (C) Population-averaged normalized filter autocorrelations $\phi(\tau)/\phi(0)$ of synaptic input currents, membrane potentials, and output spike counts obtained from the differences $E_i \left[\tilde{c}_{ii}(\tau) \right] - E_{ij} \left[\tilde{c}_{ij}(\tau) \right]$ between the corresponding auto- and cross-covariance functions shown in A and B. Thick gray curves depict autocorrelations of the kernels for synaptic currents and membrane potentials used in the simulations. Synaptic currents and membrane potentials were recorded from 10, spike trains from 2000 randomly chosen neurons. See section 5.1 for network parameters.

2000; see Kriener et al., this issue). The coherences for synaptic currents and free membrane potentials are qualitatively and quantitatively the same. This is consistent with section 2.1, showing that coherences are insensitive to linear filtering with a joint kernel. As shown in Figure 9F, the nonlinear spiking dynamics destroys input correlations to a large extent in almost all frequency bands (timescales).
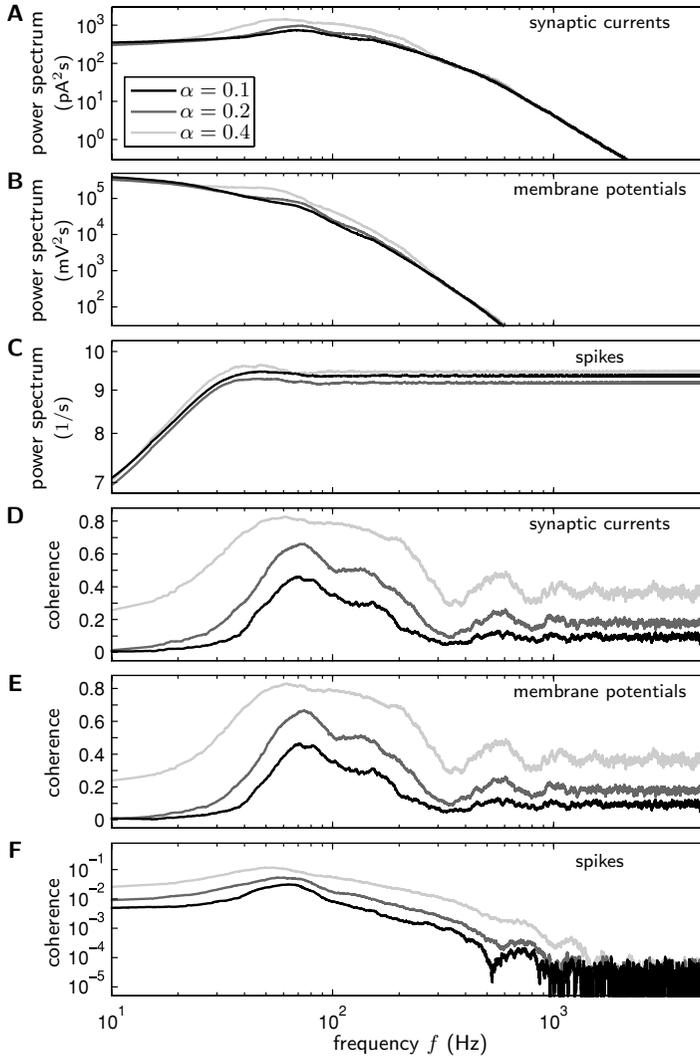
Figure 9: Estimation of common input strength (connectivity) in simulated balanced random networks (simulation time $T = 10$ s, computation step size 0.1 ms). Population-averaged power spectra (A–C) and coherences (D–F) at different signal levels: synaptic input currents (A,D), free membrane potentials (B,E), and output spike trains (C,F, bin size 0.1 ms). Different curves correspond to different network connectivities $\alpha = 0.1$ (black), 0.2 (dark gray), and 0.4 (light gray). Synaptic currents and membrane potentials were recorded from 10, spike trains from 2000 randomly chosen neurons. Spectra and coherences are smoothed by moving average (frame size 30 Hz). See section 5.1 for network parameters.

At high frequencies, the coherences between synaptic input currents and membrane potentials become constant and settle at values that are almost identical to the corresponding network connectivities α. According to section 4, high-frequency input coherences reflect the effective common input strength, which is in our case close to the connection probability α (see equation 4.27). We conclude that also in a network of integrate-and-fire neurons, high-frequency coherences can be utilized to measure the network connectivity. As shown in appendix A, this is mainly due to the fact that spike correlations (coherences) are small (see Figure 9F and Figure 10C).

If the presynaptic spike trains are described by stationary uncorrelated Poisson processes, both the input coherences and correlation coefficients recapture the common input strength. To test how far this Poisson assumption holds for the spike trains obtained by network simulations, we compare both measures quantitatively for three different connectivities, $\alpha = 0.1, 0.2$, and 0.4, in Figure 10. The plotted high-frequency coherences are obtained by averaging the coherences in the frequency range 2 kHz to 5 kHz. Both correlation coefficients and high-frequency coherences exhibit a monotonous dependence on the network connectivity α. The input coherences, however, estimate the effective common input strengths much more reliably than correlation coefficients at the level of both synaptic currents (see Figure 10A) and free membrane potentials (see Figure 10B). Correlations at the output side are strongly suppressed (see Figure 10C). Nevertheless, they still exhibit a monotonous dependence on the network connectivity (Figure 10C, not shown for coherences). Note that small sample sizes generally overestimate small coherences. The spike coherences obtained at sample size 2000 are significantly smaller than the values obtained at sample size 10 (cf. the means and error bars in Figure 10C). Therefore, the spike coherences in Figure 10C should be interpreted as upper bounds.

The network simulations show that the transmission of correlations from the input (synaptic currents, free membrane potentials) to the output side (spikes) is very weak. This is in line with several other theoretical studies on the correlation transmission by pairs of neurons (Shadlen & Newsome, 1998; Halliday, 2000; Stroeve & Gielen, 2001; Tetzlaff, Buschermöhle, Geisel, & Diesmann, 2003; Moreno-Bote & Parga, 2006). Moreover, as shown in section 4.2, spike correlations do not affect the input correlations if the network is perfectly balanced (for $K_E = gK_I$; see equation 4.18). We recently demonstrated that also for slightly unbalanced networks the effect of small spike correlations is negligible for the input correlations (see Kriener et al., this issue). Thus, as long as spike correlations are small and the synaptic input is roughly balanced, input correlations are mainly determined by the number of shared common sources, that is, the network structure. Overall our results indicate that correlations between input signals provide much more information about the underlying network structure than spike correlations.
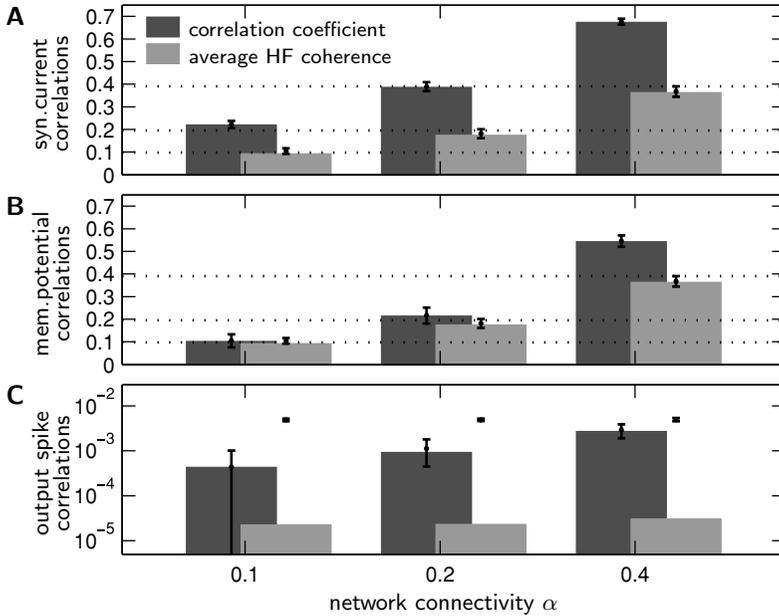
Figure 10: Correlation coefficients (dark gray bars) and averaged high-frequency (2–5 kHz) coherences (light gray bars) and their relation to the network connectivity $\alpha \in \{0.1, 0.2, 0.4\}$ for synaptic input currents (A), free membrane potentials (B), and output spikes (C, bin size 0.1 ms). Dashed horizontal lines in *A* and *B* indicate the effective common input strengths $0.098, 0.195, 0.390$ for the three connectivities α (see equation 4.27). Data obtained from network simulations (cf. Figure 9). Gray bars represent results from recordings of 10 (A, B) and 2000 (C) neurons, respectively. Error bars show statistics (mean±SD) for smaller sample sizes: 45 independent drawings of 2 (A,B) and 10 neurons (C), respectively. Small spike coherences (C, error bars not distinguishable) are systematically overestimated for small sample sizes.

6 Discussion

We summarize the main results of this study in section 6.1 and subsequently interpret our findings in the light of contemporary problems of neuroscience:

- Section 6.2 refers back to the original motivation of this work by discussing the interaction of temporally structured correlations with the timescale of the measurement process.
- There is substantial experimental evidence that neuronal correlations are modulated on short timescales. Section 6.3 argues that some of

these findings may be explained by dynamic changes in single neuron properties or the marginal spike train statistics.

- The high-frequency coherence of neuronal signals is largely unaffected by the complex network dynamics and in many applications independent of linear filter properties. This can be exploited (see section 6.4) to estimate network connectivity.
- The network models used in this study predict the magnitude of input correlations and demonstrate that the transfer of small correlation to spike output is weak. Section 6.5 relates these model predictions to the experimental literature.

6.1 Summary of Results. We analyzed how the joint statistics of linearly filtered spike trains (shot noise) depend on the statistics of the underlying point processes and the properties of the filter kernels. Although the analysis presented in section 2.1 is a straightforward generalization of standard shot-noise theory (Papoulis & Pillai, 2002), the consequences of spike train filtering (e.g., by the synapses, neurons, or the measurement technique) for the dynamics and interpretation of correlations in neuronal systems have to our knowledge never been explicitly considered.

The one-dimensional shot-noise correlation functions result from the spike train correlation functions by convolution with the deterministic filter (auto-)correlation. In consequence, standard second-order statistical measures like the variance and the covariance generally depend on the filter properties in a nontrivial way. The normalization of the covariance by the geometric mean of the variances does not compensate for this in general. Only for Poisson point processes with delta-shaped correlation function, this dependence is trivial (i.e., multiplicative). Prominently, the widely used spike count correlation coefficient depends on the bin size if the spike trains are not Poissonian, even under optimal conditions like stationarity across trials and time. Similarly, correlation coefficients between synaptic conductances, currents, or membrane potentials are modulated by the time constants of the synapses or the membranes, respectively.

The coherence, in contrast, is filter independent if each signal can be described as a simple shot-noise process that arises from a linear convolution of a single (compound) spike train with some filter kernel (e.g., spike counts). Therefore, coherence measurements often constitute a less ambiguous quantification of neuronal interactions. In this light, it is not surprising that the literature frequently refers to the zero-frequency coherence (i.e., the normalized cross-correlation area) also as the correlation coefficient. Although this definition differs from that of standard textbooks (Hollander & Wolfe, 1999; Feller, 1971), it has the advantage that this measure is not sensitive to filtering by a joint linear kernel. In many cases, the analyzed signals result from superpositions of several spike trains filtered by different kernels. Here, both the correlation coefficient and the coherence depend in general on the filter characteristics (even if the filters are linear).

Intracellularly recorded membrane currents or potentials, for example, arise from filtering of presynaptic spike trains at different synapses, which vary not only in their amplitude (weight) but also in their time constants. Since the number of synapses of a cortical neuron is large, it may be a reasonable approach to replace the individual filters by an average kernel (mean-field description). The same holds for mass signals reflecting the activity of large neuron populations (LFP, EEG). Although we did not further analyze such scenarios in this study, we conclude that there are several applications where the assumption of identical filter kernels may constitute a good approximation.

Both the correlation coefficient and the coherence generally depend on not only the joint spike train statistics but also the marginal second-order statistics of the individual point processes. It is therefore questionable whether these quantities qualify as appropriate measures for the co-relation or cooperation between two sources. This problem is difficult to address in a general context. We therefore focused on a specific type of correlations caused by overlapping presynaptic neuron populations in neural networks. Here, the relative common input strength $\alpha = v_c / v$, that is, the ratio between the compound firing rate v_c of the common sources and the total rate v, is a well-defined quantity that also corresponds to the (functional) connectivity of an underlying network. We showed that the high-frequency coherence can, under simplifying assumptions, provide a direct measure of the common input strength for a large class of point processes.

For simplicity, we based our study on the assumption that the spike train filtering is linear. While this is definitely the case for the commonly used spike count measure, it has to be investigated in how far nonlinearities, caused, for example, by shunting effects, voltage-dependent conductances, or synaptic dynamics (depression, facilitation), affect correlations between intracellularly recorded signals (synaptic currents, membrane potentials) or mass signals like local-field potential, EEG, or fMRI BOLD recordings. In general, nonlinear filtering leads to a dependence of the coherence on the filter properties.

The estimation of the network connectivity in sections 4 and 5 relies on the assumption that all synapses are reliable. Synaptic failure causes a decorrelation of inputs: if one assumes that spikes are transmitted with a probability $\rho < 1$—that both the common and the disjoint input processes are independently diluted—the common-input strength would be effectively decreased by this factor ρ. Hence, an estimation of the network connectivity by an analysis of input correlations requires knowledge of the synaptic reliability.

As pointed out in section 3.5, the presence of delay distributions is critical for our results on high-frequency coherences because they typically cause a decrease in the cross-spectra at high frequencies that is not compensated by a drop in the power spectra. On the one hand, this complicates the reconstruction of the common input strength from measured auto- and

cross-correlations. On the other hand, however, the same analysis may provide a way to estimate delay distributions from parallel intracellular recordings.

6.2 Timescale of Correlations. Spike train correlation functions and the corresponding cross-spectra are generally structured for various reasons. Depending on the measurement timescale, these correlations can be observed only in limited frequency bands. In most cases, this is a minor restriction for the experimenter measuring correlations between spike trains (spike counts) of individual neurons, because the average interspike interval of single unit recordings typically exceeds the bin size used to compute spike counts (Aertsen et al., 1989: $h = 1.5$–50 ms; Vaadia et al., 1995: 30–70 ms; Lampl et al., 1999: 1 ms; Sakurai & Takahashi, 2006: 0.1–1 ms). There are also examples in the literature where the bin size is much larger than the mean interspike interval (Zohary et al., 1994: $h = 2$ s, firing rates up to $50 \, \mathrm{s}^{-1}$). According to our results in sections 2.3 and 3.3, one can expect that the resulting spike count correlation coefficients in these cases depend on the marginal spike train statistics.

The quantification and interpretation of correlations become particularly problematic if the compound activities from large populations of neurons are compared. This is relevant for all signals reflecting synaptic inputs originating from several hundreds or thousands of presynaptic cells (e.g., synaptic currents, membrane potentials, local field potentials, optical imaging). On the one hand, the net firing rates of these superimposed presynaptic spike trains are in the range of $10^2, \ldots, 10^4 \, \mathrm{s}^{-1}$ and therefore require high recording resolutions. On the other hand, this compound spiking activity can be observed only after low-pass filtering by the synapses or the cell membranes with time constants in the range of several milliseconds. Thus, the high-frequency components of the joint activity are suppressed. We showed that the correlation coefficient cannot compensate for this, but a normalization in the frequency domain (i.e., coherence) can.

A drawback of using coherence is that correlation measures defined in the frequency domain always require some sort of time averaging (Fourier integral). Thus, time-resolved coherences can be computed only with a finite temporal resolution (see, e.g., Figure 1C). As a result correlations in the time domain may still be more appropriate (e.g., the joint PSTH; see Aertsen et al., 1989) if a high temporal resolution is desired.

6.3 Dynamics of Correlations. It is well known that correlations between spike trains can undergo dynamic modulations in relation to the experimental protocol (Aertsen et al., 1989; Vaadia et al., 1995; Grün, Diesmann, & Aertsen, 2002; Kohn & Smith, 2005; Sakurai & Takahashi, 2006). The mechanisms generating the observed changes in correlation, however, are not sufficiently understood. In the standard interpretation,

time-dependent correlations reflect the activation of different "cell assemblies" or subnetworks inducing firing rate modulations in afferents common to both target neurons. There are, however, alternative explanations. We demonstrated that modulations in the filter properties of synapses or membranes, such as changes in their time constants, can cause changes in correlation coefficients not only at the level of synaptic currents or membrane potentials but also at the level of spikes. Dendritic integration properties, for example, are governed by the amount of synaptic input (Destexhe et al., 2003). In the presence of massive synaptic bombardment, the effective membrane time constants of neurons are decreased (Kuhn et al., 2004; however cf. Waters & Helmchen, 2006). Furthermore, we showed that changes in correlations can also be caused by alterations in the presynaptic marginal second-order statistics. Even if the firing rates of common and disjoint presynaptic sources remain constant, changes in the interval statistics can induce an increase or a decrease of correlations in signals generated by the postsynaptic target cells. We pointed out that global oscillations in the presynaptic neuron populations might play an important role here. Changes in the oscillation frequency can effectively modulate the amplitude of measured correlations (see also Halliday, 2000).

In order to understand why groups of neurons synchronize or desynchronize under different stimulus conditions or in different phases of an experiment, it is essential to disentangle these different effects. Because the coherence is less sensitive to linear filtering, it may provide a tool to clarify how far changes in the neuronal filter properties contribute to the dynamics of correlations. This approach is, however, meaningful only if the modulation of the filter properties is slow compared to the length of the analysis windows used to compute time-resolved coherences. Otherwise the filters cannot be considered as time invariant, which is a necessary constraint for the coherence to become filter independent.

6.4 Revealing Network Structure from Intracellular Signals. Common presynaptic input is one of the major causes of correlated activity in neural networks. Depending on the network architecture, the presynaptic neuron populations of two or more target cells generally overlap to some extent. Spikes emitted by these common sources arrive at the target cells approximately simultaneously and give rise to more or less broadened central peaks in the cross-correlation functions of postsynaptic membrane potentials (Lampl et al., 1999) or spikes (Aertsen et al., 1989; Vaadia et al., 1995; Shadlen & Newsome, 1998; Bair et al., 2001; Kohn & Smith, 2005; Moreno-Bote & Parga, 2006). The amplitude and temporal structure of these correlations are to a large extent determined by the relative common input strength, which is closely related to the effective network connectivity, and the distribution of spike transmission delays. The measurement and analysis of common-input correlations therefore seem to be

a promising approach to study the functional structure of the underlying network.

We showed that under natural conditions, the interpretation of measured correlation functions or correlation coefficients in terms of network structure is problematic due to their dependence on the filter properties and the marginal statistics of the presynaptic spike trains. In general, this holds also for correlations measured in the frequency domain. Only under simplified conditions (identical linear filters, homogeneous spike transmission delays, uncorrelated spiking activity) can the high-frequency coherence between intracellularly recorded signals (synaptic conductances, currents, membrane potentials) be used to measure the network connectivity regardless of the network state. Here, the notion "high frequency" refers to frequencies at which the spectra of the compound input point processes become flat and are not affected by the dynamics of the system. As in real-life situations only the shot-noise spectra (but not the underlying point-process spectra) are observable, it is necessary to compute the shot-noise coherence for a broad frequency range and to find out where it approaches a constant level. As discussed in section 3.5, delay distributions impose a serious problem here: they cause a broadening of the central peak in the cross-correlation functions, thereby destroying their high-frequency components. The coherence therefore decays to zero at frequencies that roughly correspond to the inverse width of the delay distribution. Assuming a delay distribution width of about 10 ms (see Swadlow, 1998) would result in a coherence drop at about 100 Hz. Since the dynamics of cortical networks typically still occupies this frequency range, it is unlikely to find an intermediate frequency band in which the coherence is affected by neither the network dynamics nor the delay distribution. In a realistic scenario, an estimation of the network connectivity from coherences therefore requires knowledge of the delay distributions. The relation between delay distributions and input coherences could, on the other hand, be used to measure delay distributions from pairwise intracellular recordings.

There is growing experimental evidence that local cortical networks are not random (Song, Per, Reigl, Nelson, & Chklovskii, 2005). Systematic parallel intracellular recordings from neurons at different locations and potentially in different layers can help to uncover the joint connectivity statistics. Yoshimura et al. (2005) and Yoshimura and Callaway (2005), for example, utilized correlations between intracellularly recorded signals in in vitro preparations to show that specific fine-scale subnetworks are embedded into larger-scale functional columns. Our findings can be used to verify and extend these studies also for in vivo preparations.

6.5 Correlations in Cortical Networks. The network model in section 5 predicts that the input correlations are predominantly determined by the network connectivity α (see also Kriener et al., this issue). According to

anatomical data (Abeles, 1991; Braitenberg & Schüz, 1991; Hellwig, 2000), we would therefore expect average input correlations of about 0.1 in a cortical volume of roughly 1 mm^3. For the cat visual cortex, Lampl et al. (1999) reported a broad range of membrane potential correlations with a mean of about 0.4. There are several possible reasons for this deviation from our model. First, as indicated above, the topology of local cortical networks differs from a random connectivity (Song et al., 2005). Second, the distributions of in-degrees (number of inputs per neuron) are certainly much broader than assumed in this study, and the probability of finding a common presynaptic neuron shared by two (observed) target cells may significantly differ from chance level α^2. Third, our network model does not exhibit nonstationarities in time, which can arise, for example, from the local dynamics or from time-dependent external inputs. In section 4, we showed that such nonstationarities can effectively modulate the amplitude of correlations. Fourth, spatially correlated external inputs from other cortical or subcortical areas were neglected (see Roy & Alloway, 2001; Bruno & Sakmann, 2006). The distribution of input correlation coefficients would certainly be wider and shifted toward higher values if these different aspects were taken into account.

The results of sections 4 and 5 and those of several other theoretical studies (Shadlen & Newsome, 1998; Stroeve & Gielen, 2001; Tetzlaff et al., 2003; Moreno-Bote & Parga, 2006; de la Rocha, Doiron, Shea-Brown, Kresimir, & Reyes, 2007; Kriener et al., this issue) suggest that the transmission of small input correlations to output spike correlations is rather weak. Even for networks with connectivities of 0.4 (and therefore input correlations of 0.4), we observe in section 5 average output correlation coefficients on the order of 10^{-3}. In contrast, many experimental studies reported that cortical neurons exhibit stimulus-unspecific spike correlation coefficients of the order of 0.1 or higher (Zohary et al., 1994; Vaadia et al., 1995; Gawne & Richmond, 1993; Shadlen & Newsome, 1998; Bair et al., 2001). This disagreement is to some extent presumably also due to the fact that several features of cortical connectivity have been neglected in our model (see above). Furthermore, in the experimental studies mentioned here, spikes from different units were recorded with a single electrode. Thus, the observed correlations refer to neurons within a radius of not more than 50 μm (Henze et al., 2000; Sakurai & Takahashi, 2006). Stimulus-unspecific spike correlations (shared input correlations) of neurons recorded on different electrodes are typically weaker (Ts'o, Gilbert, & Wiesel, 1986; Gochin, Miller, Gross, & Gerstein, 1991; Vaadia & Aertsen, 1992). Our model in section 5 does not account for neighborhood relationships between neurons and therefore cannot reproduce distance dependencies of correlations. It rather describes an average picture at a scale of about 1 mm^3. While the apparent discrepancy between experiment and model results remains a puzzle, at the spatial scale discussed in this article, the predicted small average spike correlation seems plausible.

Appendix A: Estimation of the Common Input Strength for Correlated Spike Trains

In section 3.2 we assumed that common and disjoint processes are mutually uncorrelated. However, the results of section 3.4 can be generalized to the case of correlated spiking—for $\tilde{\psi}_{pq}(\tau) \neq 0$ ($p, q \in \{c, d_i, d_j\}$). For Poisson processes with delta-type correlations, the covariance functions read

$$\tilde{\psi}_{pq}(\tau) = r_{pq}\sqrt{v_p v_q}\,\delta(\tau). \tag{A.1}$$

Here, r_{pq} denotes the pairwise correlation coefficient between the processes $\xi_p(t)$ and $\xi_q(t)$. The corresponding spectra are constant

$$\tilde{\Psi}_{pq}(\omega) = r_{pq}\sqrt{v_p v_q}. \tag{A.2}$$

We can generalize this to a broader class of processes for which equation A.2 still holds for large frequencies,

$$\lim_{\omega\to\infty} \tilde{\Psi}_{pq}(\omega) = r_{pq}\sqrt{v_p v_q}. \tag{A.3}$$

Similar to section 3.1, let us assume that the disjoint processes have identical autocorrelations ($\tilde{\psi}_{d_i d_i}(\tau) = \tilde{\psi}_{d_j d_j}(\tau)$) and therefore identical rates v_d. For simplicity, we further assume that all correlation coefficients are identical ($r = r_{pq}\ \forall\{p, q\}$). In this case, the high-frequency coherence between the input signals

$$\xi_{i/j}(t) = \xi_c(t) + \xi_{d_{i/j}}(t) \tag{A.4}$$

becomes

$$
\begin{aligned}
\lim_{\omega\to\infty} \kappa(\omega) &= \lim_{\omega\to\infty} \frac{\tilde{\Psi}_{cc}(\omega) + \tilde{\Psi}_{d_i d_j}(\omega) + \tilde{\Psi}_{cd_j}(\omega) + \tilde{\Psi}_{d_i c}(\omega)}{\tilde{\Psi}_{cc}(\omega) + \tilde{\Psi}_{d_i d_i}(\omega) + \tilde{\Psi}_{cd_j}(\omega) + \tilde{\Psi}_{d_i c}(\omega)} \\
&= \frac{v_c + r v_d + 2r\sqrt{v_c v_d}}{v_c + v_d + 2r\sqrt{v_c v_d}}.
\end{aligned}
\tag{A.5}
$$

With $v_c = \alpha v$ and $v_d = (1-\alpha)v$, this can be written as

$$\lim_{\omega\to\infty} \kappa(\omega) = \alpha\frac{1 + r\alpha^{-1}(1-\alpha) + 2r\sqrt{\alpha^{-1}(1-\alpha)}}{1 + 2r\sqrt{\alpha(1-\alpha)}}. \tag{A.6}$$

Thus, by solving equation A.6 for α, the common input strength can be estimated from the high-frequency coherence if the spike correlation coefficient r is known. Note that according to equation A.3, r can be

determined by measuring the high-frequency coherences of the spike signals: $\lim_{\omega \to \infty} |\check{\Psi}_{pq}(\omega)| / \sqrt{\check{\Psi}_{pp}(\omega) \check{\Psi}_{qq}(\omega)}$.

Appendix B: Count Covariances for Jittered Correlations ─────────

Here we derive the spike count correlation coefficient r_{ij} for two Poissonian spike trains with rectangular and gaussian cross-covariance function. The results are shown in Figure 5.

B.1 Rectangular Cross-Correlations. For a rectangular covariance function,

$$\tilde{\psi}_{ij}(\tau)(\tau) = \begin{cases} \dfrac{\nu_c}{2\sigma} & -\sigma \le \tau \le \sigma, \\ 0 & \text{else} \end{cases} \tag{B.1}$$

the count covariance is according to equation 2.15 given by

$$\tilde{c}_{ij} = \nu_c \begin{cases} \dfrac{1}{2\sigma} h^2 & h \le \sigma \\ \left(h - \dfrac{\sigma}{2} \right) & h > \sigma \end{cases}. \tag{B.2}$$

After normalizing $\tilde{c}_{ij}$ by the count variance $\tilde{c}_{ii} = \nu h$ and with $\alpha = \nu_c / \nu$, the correlation coefficient reads

$$r_{ij} = \alpha \begin{cases} \dfrac{1}{2\sigma} h & h \le \sigma \\ \left(1 - \dfrac{\sigma}{2h} \right) & h > \sigma \end{cases}. \tag{B.3}$$

Figure 5A shows how r_{ij} depends on the bin size h for $\sigma = 2\,\text{ms}$ and $16\,\text{ms}$ and $\alpha = 0.5$.

B.2 Gaussian Cross-Correlations. If the spike covariance function has a gaussian shape,

$$\tilde{\psi}_{ij}(\tau) = n(\tau, \sigma) := \frac{\nu_c}{\sqrt{2\pi\sigma^2}} \exp\left(-\frac{\tau^2}{2\sigma^2} \right), \tag{B.4}$$

the count covariance becomes

$$\tilde{c}_{ij} = 2\nu_c \left[\frac{h}{2} \operatorname{erf}\left(\frac{h}{\sqrt{2}\sigma} \right) - \sigma^2 \left[n(0, \sigma) - n(h, \sigma) \right] \right], \tag{B.5}$$

where erf($\cdot$) denotes the error function

$$\mathrm{erf}(x) = \frac{2}{\sqrt{\pi}} \int_0^x \mathrm{d}x' \ \exp(-x'^2). \tag{B.6}$$

Thus, the count correlation coefficient is given by

$$r_{ij} = \alpha \left[\mathrm{erf}\left(\frac{h}{\sqrt{2}\sigma}\right) - \frac{2\sigma^2}{h} \left[n(0, \sigma) - n(h, \sigma)\right] \right]. \tag{B.7}$$

Its bin-size dependence is illustrated in Figure 5B ($\sigma = 2\,\mathrm{ms}$ and $16\,\mathrm{ms}$, $\alpha = 0.5$).

Acknowledgments

References

Abeles, M. (1991). *Corticonics: Neural circuits of the cerebral cortex*. Cambridge: Cambridge University Press.

Aertsen, A., & Arndt, M. (1993). Response synchronization in the visual cortex. *Curr. Opin. Neurobiol., 3*, 586–594.

Aertsen, A., Gerstein, G., Habib, M., & Palm, G. (1989). Dynamics of neuronal firing correlation: Modulation of "effective connectivity." *J. Neurophysiol., 61*(5), 900–917.

Bair, W., Zohary, E., & Newsome, W. (2001). Correlated firing in macaque visual area MT: Time scales and relationship to behavior. *J. Neurosci., 21*(5), 1676–1697.

Bienenstock, E. (1995). A model of neocortex. *Network: Comput. Neural Systems, 6*, 179–224.

Braitenberg, V., & Schüz, A. (1991). *Anatomy of the cortex: Statistics and geometry*. Berlin: Springer-Verlag.

Brown, E. N., Kaas, R. E., & Mitra, P. P. (2004). Multiple neural spike train data analysis: State-of-the-art and future challenges. *Nat. Neurosci., 7*(5), 456–461.

Brunel, N. (2000). Dynamics of sparsely connected networks of excitatory and inhibitory spiking neurons. *J. Comput. Neurosci., 8*(3), 183–208.

Brunel, N., & Hakim, V. (1999). Fast global oscillations in networks of integrate-and-fire neurons with low firing rates. *Neural Comput., 11*(7), 1621–1671.

Bruno, R. M., & Sakmann, B. (2006). Cortex is driven by weak but synchronously active thalamocortical synapses. *Science, 312*, 1622–1627.

Cox, D. R. (1962). *Renewal theory*. London: Methuen.

Daley, D. J., & Vere-Jones, D. (2005). *An introduction to the theory of point processes, Vol. 1: Elementary theory and methods* (2nd ed.). New York: Springer.

De la Rocha, J., Doiron, B., Shea-Brown, E., Kresimir, J., & Reyes, A. (2007). Correlation between neural spike trains increases with firing rate. *Nature, 448*(16), 802–807.

Destexhe, A., & Paré, D. (1999). Impact of network activity on the integrative properties of neocortical pyramidal neurons in vivo. *J. Neurophysiol., 81*(4), 1531–1547.

Destexhe, A., Rudolph, M., & Pare, D. (2003). The high-conductance state of neocortical neurons in vivo. *Nat. Rev. Neurosci., 4*, 739–751.

Eckhorn, R., Bauer, R., Jordan, W., Brosch, M., Kruse, W., Munk, M., et al. (1988). Coherent oscillations: A mechanism of feature linking in the visual cortex? *Biol. Cybern., 60*, 121–130.

Fano, U. (1947). Ionization yield of radiations. II. The fluctuations of the number of ions. *Phys. Rev., 72*(1), 26–29.

Feller, W. (1971). *An introduction to probability theory and its applications* (2nd ed.). New York: Wiley.

French, C. C., & Beaumont, J. G. (1984). A critical review of EEG coherence studies of hemisphere function. *Int. J. Psychophysiol., 1*(3), 241–254.

Fries, P., Reynolds, J., Rorie, A., & Desimone, R. (2001). Modulation of oscillatory neuronal synchronization by selective visual attention. *Science, 291*(5508), 1560–1563.

Gawne, T. J., & Richmond, B. J. (1993). How independent are the messages carried by adjacent inferior temporal cortical neurons? *J. Neurosci., 13*(7), 2758–2771.

Gerstner, W., & Kistler, W. (2002). *Spiking neuron models: Single neurons, populations, plasticity*. Cambridge: Cambridge University Press.

Gochin, P. M., Miller, E. K., Gross, C. G., & Gerstein, G. L. (1991). Functional interactions among neurons in inferior temporal cortex of the awake macaque. *Exp. Brain Res., 84*(3), 505–516.

Gray, C. M. (1994). Synchronous oscillations in neuronal systems: Mechanisms and functions. *J. Comput. Neurosci., 1*, 11–38.

Gray, C. M., König, P., Engel, A. K., & Singer, W. (1989). Oscillatory responses in cat visual cortex exhibit inter-columnar synchronization which reflects global stimulus properties. *Nature, 338*, 334–337.

Gray, C. M., & Singer, W. (1989). Stimulus-specific neuronal oscillations in orientation columns of cat visual cortex. *Proc. Natl. Acad. Sci. USA, 86*, 1698–1702.

Grün, S., Diesmann, M., & Aertsen, A. (2002). "Unitary events" in multiple single-neuron spiking activity. II. Non-stationary data. *Neural Comput., 14*(1), 81–119.

Halliday, D. M. (2000). Weak, stochastic temporal correlation of large scale synaptic input is a major determinant of neuronal bandwidth. *Neural Comput., 12*, 693–707.

Hasson, U., Nir, Y., Levy, I., Fuhrmann, G., & Malach, R. (2004). Intersubject synchronization of cortical activity during natural vision. *Science, 303*, 1634–1640.

Hayon, G., Abeles, M., & Lehmann, D. (2004). Modeling compositionality by dynamic binding of synfire chains. *J. Comput. Neurosci., 17*, 179–201.

Hellwig, B. (2000). A quantitative analysis of the local connectivity between pyramidal neurons in layers 2/3 of the rat visual cortex. *Biol. Cybern., 2*(82), 111–121.

Henze, D., Borhegyi, Z., Csicsvari, J., Mamiya, A., Harris, K., & Buzsaki, G. (2000). Intracellular features predicted by extracellular recordings in the hippocampus in vivo. *J. Neurophysiol., 1*(84), 390–400.

Hollander, M., & Wolfe, D. (1999). *Nonparametric statistical methods* (2nd ed.). New York: Wiley.

Jarvis, M. R., & Mitra, P. P. (2001). Sampling properties of the spectrum and coherency of sequences of action potentials. *Neural Comput., 13*, 717–749.

Kohn, A., & Smith, M. A. (2005). Stimulus dependence of neuronal correlations in primary visual cortex of the macaque. *J. Neurosci., 25*(14), 3661–3673.

Kriener, B., Tetzlaff, T., Aertsen, A., Diesmann, M., & Rotter, S. (2008). Correlations and population dynamics in cortical networks. *Neural Comput., 20*(9), 2185–2226.

Kuhn, A., Aertsen, A., & Rotter, S. (2003). Higher-order statistics of input ensembles and the response of simple model neurons. *Neural Comput., 15*(1), 67–101.

Kuhn, A., Aertsen, A., & Rotter, S. (2004). Neuronal integration of synaptic input in the fluctuation-driven regime. *J. Neurosci., 24*(10), 2345–2356.

Lampl, I., Reichova, I., & Ferster, D. (1999). Synchronous membrane potential fluctuations in neurons of the cat visual cortex. *Neuron, 22*, 361–374.

Logothetis, N. K., Pauls, J., Augath, M., Trinath, T., & Oeltermann, A. (2001). Neurophysiological investigation of the basis of the fMRI signal. *Nature, 412*, 150–157.

Mikula, S., & Niebur, E. (2003). The effects of input rate and synchrony on a coincidence detector: Analytical solution. *Neural Comput., 15*, 539–547.

Moreno-Bote, R., & Parga, N. (2006). Auto- and crosscorrelograms for the spike response of leaky integrate-and-fire neurons with slow synapses. *Phys. Rev. Lett., 96*, 028101.

Mukamel, R., Gelbard, H., Arieli, A., Hasson, U., Fried, I., & Malach, R. (2005). Coupling between neuronal firing, field potentials, and fMRI in human auditory cortex. *Science, 309*(5736), 951–954.

Oviedo, H., & Reyes, A. D. (2002). Boosting of neuronal firing evoked with asynchronous and synchronous inputs to the dendrite. *Nat. Neurosci., 5*(3), 261–266.

Palm, G., Aertsen, A. M. H. J., & Gerstein, G. L. (1988). On the significance of correlations among neuronal spike trains. *Biol. Cybern., 59*, 1–11.

Papoulis, A., & Pillai, S. U. (2002). *Probability, random variables, and stochastic processes* (4th ed.). New York: McGraw-Hill.

Perkel, D. H., Gerstein, G. L., & Moore, G. P. (1967a). Neuronal spike trains and stochastic point processes. I. The single spike train. *Biophys. J., 7*(4), 391–418.

Perkel, D. H., Gerstein, G. L., & Moore, G. P. (1967b). Neuronal spike trains and stochastic point processes. II. Simultaneous spike trains. *Biophys. J., 7*(4), 419–440.

Pipa, G., van Vreeswijk, C., & Grün, S. (2008). *Impact of spike-train autostructure on probability distribution of joint-spike events*. Manuscript submitted for publication.

Priestley, M. (1983). *Spectral analysis and time series*. Orlando, FL: Academic Press.

Prut, Y., Vaadia, E., Bergman, H., Haalman, I., Hamutal, S., & Abeles, M. (1998). Spatiotemporal structure of cortical activity: Properties and behavioral relevance. *J. Neurophysiol., 79*(6), 2857–2874.

Riehle, A., Grün, S., Diesmann, M., & Aertsen, A. (1997). Spike synchronization and rate modulation differentially involved in motor cortical function. *Science, 278*, 1950–1953.

Rotter, S., Riehle, A., Rodriguez Molina, V., Aertsen, A., & Nawrot, M. P. (2005). *Different time scales of spike train variability in motor cortex*. Abstract Viewer and Itinerary Planner, Society for Neuroscience, Washington, DC, no. 276.7.

Roy, S. A., & Alloway, K. D. (2001). Coincidence detection or temporal integration? What the neurons in somatosensory cortex are doing. *J. Neurosci., 21*(7), 2462–2473.

Rudolph, M., & Destexhe, A. (2001). Correlation detection and resonance in neuronal systems with distributed noise sources. *Phys. Rev. Lett., 86*(16), 3662–3665.

Sakurai, Y., & Takahashi, S. (2006). Dynamic synchrony of firing in the monkey prefrontal cortex during working-memory tasks. *J. Neurosci., 6*(40), 10141–10153.

Salinas, E., & Sejnowski, T. J. (2000). Impact of correlated synaptic input on output firing rate and variability in simple neuronal models. *J. Neurosci., 20*(16), 6193–6209.

Shadlen, M. N., & Newsome, W. T. (1998). The variable discharge of cortical neurons: Implications for connectivity, computation, and information coding. *J. Neurosci., 18*(10), 3870–3896.

Shaw, J. C. (1984). Correlation and coherence analysis of the EEG: A selective tutorial review. *Int. J. Psychophysiol., 1*(3), 255–266.

Singer, W., Gray, C., Engel, A., & König, P. (1988). Spatio-temporal distribution of stimulus-specific oscillations in the cat visual cortex II: Global interactions. *Soc. Neurosci. Abstr., 14*, 899.

Softky, W. R., & Koch, C. (1993). The highly irregular firing of cortical cells is inconsistent with temporal integration of random EPSPs. *J. Neurosci., 13*(1), 334–350.

Song, S., Per, S., Reigl, M., Nelson, S., & Chklovskii, D. (2005). Highly nonrandom features of synaptic connectivity in local cortical circuits. *Public Library of Science, Biology, 3*(3), 0507–0519.

Stroeve, S., & Gielen, S. (2001). Correlation between uncoupled conductance-based integrate-and-fire neurons due to common and synchronous presynaptic firing. *Neural Comput., 13*(9), 2005–2029.

Swadlow, H. A. (1998). Neocortical efferent neurons with very slowly conducting axons: Strategies for reliable antidromic identification. *J. Neurosci. Methods, 79*, 131–141.

Tetzlaff, T., Aertsen, A., & Diesmann, M. (2005). Time-scale dependence of inter-neuronal spike correlations. In *Proceedings of the 30th Göttingen Neurobiology Conference*. Available online at http://www.neuroanatomie.uni-goettingen.de/neurobio_archiv/2005/pdf/Proceedings-Goettingen2005/pdf.

Tetzlaff, T., Buschermöhle, M., Geisel, T., & Diesmann, M. (2003). The spread of rate and correlation in stationary cortical networks. *Neurocomputing, 52–54*, 949–954.

Ts'o, D. Y., Gilbert, C. D., & Wiesel, T. N. (1986). Relationships between horizontal interactions and functional architecture in cat striate cortex as revealed by cross-correlation analysis. *J. Neurosci., 6*(4), 1160–1170.

Tuckwell, H. C. (1988). *Introduction to theoretical neurobiology*. Cambridge: Cambridge University Press.

Vaadia, E., & Aertsen, A. (1992). Coding and computation in the cortex: Single-neuron activity and cooperative phenomena. In A. Aertsen & V. Braitenberg (Eds.), *Information processing in the cortex: Experiments and theory* (pp. 81–121). Berlin: Springer-Verlag.

Vaadia, E., Haalman, I., Abeles, M., Bergman, H., Prut, Y., Slovin, H., et al. (1995). Dynamics of neuronal interactions in monkey cortex in relation to behavioural events. *Nature, 373*(6514), 515–518.

van Vreeswijk, C., Abbott, L., & Ermentrout, G. (1994). When inhibition not excitation synchronizes neural firing. *J. Comput. Neurosci., 1*, 313–321.

Waters, J., & Helmchen, F. (2006). Background synaptic activity is sparse in neocortex. *J. Neurosci., 26*(32), 8267–8277.

Weiss, S., & Mueller, H. M. (2003). The contribution of EEG coherence to the investigation of language. *Brain Lang., 85*(2), 325–345.

Yoshimura, Y., & Callaway, E. (2005). Fine-scale specificity of cortical networks depends on inhibitory cell type and connectivity. *Nat. Neurosci., 8*(11), 1552–1559.

Yoshimura, Y., Dantzker, J., & Callaway, E. (2005). Excitatory cortical neurons form fine-scale functional networks. *Nature, 433*(24), 868–873.

Zohary, E., Shadlen, M. N., & Newsome, W. T. (1994). Correlated neuronal discharge rate and its implications for psychophysical performance. *Nature, 370*, 140–143.

This article has been cited by:

1. Birgit Kriener, Tom Tetzlaff, Ad Aertsen, Markus Diesmann, Stefan Rotter. 2008. Correlations and Population Dynamics in Cortical Networks. *Neural Computation* **20**:9, 2185-2226. [Abstract] [PDF] [PDF Plus]